Tectono-thermal Evolution of a Distal Rifted Margin: Constraints From the Calizzano Massif (Prepiedmont-Briançonnais Domain, Ligurian Alps)

DOI:10.1002/2017TC004634

Tectono-thermal evolution of a distal rifted margin: constraints from the Calizzano Massif (Prepiedmont-Briançonnais domain, Ligurian Alps)

Alessandro Decarlis [1, 2], Maria Giuditta Fellin [3], Matteo Maino [4], Simona Ferrando [1], Gianreto Manatschal [2], Laura Gaggero [5], Silvio Seno [4] , Finlay M. Stuart [6] & Marco Beltrando [1]†

[1] Dipartimento di Scienze della Terra, Università degli Studi di Torino, Via Valperga Caluso, 35, 10125 Torino (I).
[2] EOST/IPGS Universitè de Strasbourg, Rue Blessig, 1, F-67084 Strasbourg Cedex (F).
[3] Department of Earth sciences, ETH Zurich, Clausiusstrasse 25, 8092 Zurich (CH).
[4] Dipartimento di Scienze della Terra e dell'Ambiente, Università degli Studi di Pavia, Via Ferrata 1, 27100 Pavia (I).
[5] Dipartimento di Scienza della Terra dell'Ambiente e della Vita, Università di Genova, Corso Europa 26, 16132 Genova (I)
[6] Isotope Geosciences Unit, SUERC, Scottish Enterprise and Technology Park, Rankine Avenue, East Kilbride G750QF (UK)

Corresponding Author: Decarlis Alessandro: aledec@tin.it

Keywords: Heating-cooling cycles; Distal rifted margin thermal evolution; Ligurian Alps; Zircon fission tracks; Zircon (U-Th)/He.

ABSTRACT

The thermal evolution of distal domains along rifted margins is at present poorly constrained. In this study, we show that a thermal pulse, most likely triggered by lithospheric thinning and asthenospheric rise, is recorded at upper crustal levels and may also influence the diagenetic processes in the overlying sediments, thus representing a critical aspect for the evaluation of hydrocarbon systems. The thermal history of a distal sector of the Alpine Tethys rifted margin preserved in the Ligurian Alps (Case Tuberto-Calizzano unit) is investigated with thermochronological methods and petrologic observations. The studied unit is composed of a polymetamorphic basement and a sedimentary cover, providing a complete section through the pre-, syn- and post-rift system. Zircon fission-track analyses on basement rocks samples suggest that temperatures exceeding ~240±25 °C were reached before ~150-160 Ma (Upper Jurassic) at few kilometres depth. Neo-formation of green biotite, stable at temperatures of ~350 to 450°C, was syn-kinematic with this event. The tectonic setting of the studied unit suggests that the heating-cooling cycle took place during the formation of the distal rifted margin and terminated during Late Jurassic (150-160 Ma). Major crustal and lithospheric thinning likely promoted high geothermal gradients (~60-90°C/km) and triggered the

circulation of hot, deep-seated fluids along brittle faults, causing the observed thermal anomaly. Our results suggest that rifting can generate thermal perturbations at relatively high temperatures (between ~240 and 450°C) at less than 3 km depth in the distal domains during major crustal thinning preceding breakup and onset of seafloor spreading.

1 INTRODUCTION

The tectonic evolution of rift systems is characterized by markedly different dynamics occurring at proximal and distal margins [e.g. *Sutra* et al*.,* 2013*; Tugend* et al*.,* 2014 cum ref.]. The passage from un-thinned to thinned crustal domains marks a major change in timing and modality of the rift style across rifted margins [see *Mohn* et al*.,* 2012 *cum ref*]. The process of rift localization leads to the quiescence of tectonically active areas placed over thick continental crust in the proximal parts of the margins and to the activation of narrow sectors in which the crust becomes severely thinned (i.e. future distal margins). During final rifting, the deformation between lower and upper crust becomes "coupled" [see *Sutra et al.,* 2013], generating new fluid circulation patterns [*Incerpi* et al., 2017]. The circulation of hydrothermal fluids is typically associated with anomalous thermal gradients that lead to characteristic syn-rift heating/cooling cycles affecting the whole crustal section in the distal margin [*Beltrando* et al., 2015; *Seymour* et al., 2016]. Remnants of fossil rifted margins, exposed inside orogenic belts, may provide an opportunity to directly investigate and evaluate the character of syn-rift heating events in the case the syn-orogenic metamorphism never exceed the maximum temperatures reached during rifting.

In this study we use two thermochronometric systems, Zircon Fission Tracks (ZFT) and Zircon (U-Th)/He (ZHe) to investigate the syn-rift heating-cooling cycle at the distal rifted margin of the Alpine Tethys, which is one of the world's best fossil analogues for a magma-poor rifted margin [e.g. *Manatschal and Bernoulli*, 1999; *Manatschal*, 2004; *Mohn et al.*, 2012; *Decarlis et al.*, 2015; *Haupert et al.*, 2016]. Here we report new data that enable documentation of the thermal history of the Case Tuberto-Calizzano unit in the Ligurian Alps (Fig. 1), which belong to the distal European margin of the Alpine Tethys system [*Decarlis et al.*, 2013; 2015]. This unit only experienced low grade Alpine metamorphism [*Desmons et al.,* 1999a; *Seno et al.*, 2005a] thus it offers a rare "window" into the thermal evolution of the ancient distal margin. The goal of this paper is to decipher the local temperature conditions reached in the basement during the thermal pulse and the time-window when it was active a few kilometers beneath syn-rift sediments.

2 GEOLOGICAL SETTING

2.1 Alps orogeny and insights on Alpine Tethys rift

The Western and Central sectors of the alpine chain (Fig. 1), which straddle the Italian, French and Swiss borders, preserve the most indicative remnants of the Alpine Tethys rifted margins that survived the subsequent orogenic overprint. The Mesozoic Alpine rifting became active in the Early Jurassic [*Lemoine and Trümpy,* 1987; *Froitzheim and Manatschal*, 1996], leading to the separation of the European plate (North to North-west) from the Adria microplate (South to South-west; formerly part of Africa; Fig. 2) and to the formation of the Piedmont-Ligurian Ocean during Early Cretaceous [*Handy et al.,* 2010 *cum ref.*]. It followed the onset of convergence/subduction in Late Cretaceous and the continental collision during Tertiary times [see de *Graciansky et al.,* 2011].

The tectono-sedimentary evolution of the Alpine Tethys margins has been discussed by several studies [*e.g. Masini et al.,* 2013; *Decarlis et al.*, 2015], suggesting that the Jurassic rifting was the result of polyphase tectonics including:

(i) Stretching phase (Hettangian-Sinemurian) leading to the formation of widely distributed half-graben structures over only slightly extended 25 to 30 km thick continental crust.

(ii) Thinning phase (Pliensbachian-Toarcian) occurring only in a narrower area corresponding to the future distal margin.

(iii) Hyper-extension phase during which crustal and mantle rocks have been exhumed along detachment fault(s) at the seafloor.

During the final phase of hyperextension and exhumation, distal margins can be subdivided in upper plate (hanging-wall of the exhumation system) and lower plate [*Haupert et al*., 2016; *Decarlis et al.*, in press; Fig. 2]. Stratigraphic and structural data reported by *Lemoine et al.* [1987], *Decarlis et al.* [2015] and *Haupert et al.* [2016] showed that in the present-day Alps, the Provençal, Dauphinois and Upper Austroalpine units (Fig. 2) represent remnants of the former proximal margins, whereas the internal European units and Lower Austroalpine units are derived from the former distal margin. At present, there is a general agreement that the internal European margin and the Austroalpine were the former upper and lower plate margin, respectively. The evolution of the upper plate is defined by a strong uplift and erosion on the Briançonnais margin, while the Prepiedmont (object of the present paper) and Piedmont domains were drowned. The Ligurian, Penninic and Lower Austroalpine units represent the exhumed domain that was physically generated (exhumed) from Middle Jurassic onwards.

2.2 Ligurian Alps

The Ligurian Alps are located at the southwestern end of the Western Alps arc, towards the transition with the Northern Apennine [*Vanossi, 1991; Maino et al.*, 2013; *Decarlis et al.,* 2014]. They consist of a Variscan basement and of a Permian to Cenozoic sedimentary cover that were originally part of the palaeo-European margin, belonging to the Briançonnais-Prepiedmont domains (Figs. 1D, 2B). The Briançonnais domain was uplifted and eroded during rifting [*Claudel and Dumont*, 1999; *Decarlis and Lualdi*, 2008] as attested by a major syn-rift sedimentary hiatus. Conversely, the Prepiedmont domain displays a continuous clastic syn-rift sequence [*Decarlis and Lualdi*, 2011; *Decarlis et al.*, 2015]. From Late Cretaceous, as a consequence of the convergence and subsequent collision between the European and Adria plates, these rocks were buried and juxtaposed against remnants of exhumed subcontinental mantle, now exposed within the Voltri Massif [e.g. *Bonini et al.*, 2010; *Capponi and Crispini*, 2002]. The Briançonnais and Prepiedmont units experienced different Alpine metamorphic overprints (from anchizone to blueschist facies depending on their original position along the margin) [*Messiga et al.*, 1981; *Desmons et al.,* 1999a, 1999b; *Seno et al.*, 2005a], and since the Oligocene they were exhumed to upper crustal levels [*Seno et al.,* 2005a; 2005b; *Maino et al.*, 2012a].

The object of this study is the Case Tuberto-Calizzano unit that belongs to the Prepiedmont domain (Fig. 2). It was treated in literature as a separate stack formed by the Case Tuberto unit (Permian and Mesozoic covers) [*Dallagiovanna et al.*, 1984] and the Calizzano massif (basement unit) [*Airoldi*, 1937] until local evidence for stratigraphic continuity was reported by *Dallagiovanna* [1988] and *Cortesogno et al.* [1998]. This unit is interpreted as the more external of the whole Prepiedmont domain on the basis of both its position across the nappe pile and its stratigraphic content [*Vanossi*, 1991]. In a general section across the former rifted margin (Fig. 2), its location would correspond to the boundary between the uplifted Briançonnais domain and the submerged Prepiedmont domain.

2.3 Case Tuberto-Calizzano unit: stratigraphic outline

The "Calizzano massif" rests on the highest structural levels within the Briançonnais nappe stack, bounded downwards by a SW dipping tectonic contact [*Dallagiovanna* et al.*,* 1984] (Fig. 1C, 3). The massif preserves evidence of a protracted Palaeozoic evolution in the Gneiss-Amphibolite Complex [*e.g. Gaggero* et al., 2004], wherein Middle-Late Cambrian bimodal effusive tholeiitic and transitional basalts and acidic calcalkaline volcanites associated with pelitic, psammitic and arenitic sediments were intruded by Late Cambrian-Early Ordovician granitoids (commonly labelled 'Orthogneiss 1'), which underwent Early Ordovician metamorphic re-equilibration under eclogite (760°C, >1.7 GPa) to amphibolite (680°C, >1.1 GPa) facies conditions [e.g. *Cortesogno* et al., 1993; *Desmons* et al., 1999a; *Gaggero* et al., 2004].

The subsequent intrusion of large granitic bodies ('Orthogneiss 2') and minor gabbros at ca. 470-460 Ma was then followed by a Variscan medium to low-P amphibolite facies (ca. 600-650°C, 0.4-0.6 GPa) schistogenous event at ca. 330 Ma [*Gaggero* et al., 2004] and by a folding event with production of actinolite+chlorite, greenschist-facies mineral assemblage (actinolite+chlorite) along axial planes of open folds [*Gaggero* et al., 2004]. In the study area and in similar basement units (Nucetto and Savona massifs), Lower Carboniferous-Early Permian (327-274 Ma) ^{40}Ar-^{39}Ar and Rb/Sr ages [*Del Moro* et al*.,* 1982a; *Barbieri* et al*.,* 2003] and local occurrence of Permian lava flows resting directly on the lower Palaeozoic metamorphic basement [*Dallagiovanna et al*., 2009; *Maino* et al., 2012b] demonstrate that this folding event was followed by exhumation to shallow crustal levels.

The basement is locally overlain by Middle Permian pyroclastites and tuffs (Melogno porphyroids Fm: about 150 m), followed by the Upper Permian to Lower Triassic conglomerates and sandstones (Monte Pianosa Formation and Ponte di Nava Quartzite: about 150 m) and by Middle Triassic to Lower Jurassic carbonate rocks (San Salvatore Dolostone and Rocca Prione Fm, M. Arena Dolostone, Veravo Limestone, Rocca Liverna' Limestone, 250 m in thickness) [*Vanossi*, 1991]. As reported by Dallagiovanna (1988), the Upper Permian to Triassic *p.p.* succession may be locally replaced by some tens of metres of polymictic breccias and conglomerates sampling the aformentioned lithologies (Monte Pennino Breccia) [*Crozi*, 1998].

The Triassic-Jurassic successions grade upward into a poorly dated sedimentary sequence, which is commonly ascribed to the Jurassic-Eocene (Scravaion schists) sedimentary cycle [*Vanossi*, 1970; *Dallagiovanna & Seno*, 1984; *Vanossi et al.,* 1986]. Notably, this Mesozoic and Cenozoic sedimentary succession has been mainly inferred [*Dallagiovanna* et al., 1984] to be a composite section due to the lack of a continuous field transect in which the different terrains are juxtaposed by indisputable stratigraphic boundaries. Its overall stratigraphic setting has been mostly determined by comparison with adjacent units of the Briançonnais and Prepiedmont domains. Thus, the total thickness of the Case Tuberto sedimentary cover (estimated as about 600 m) [*Vanossi,* 1991] should be considered a rough estimate, due to a number of factors, including: (1) the above-described stratigraphic uncertainty, (2) the occurrence of Alpine low-T fabrics related to solution-precipitation processes, which likely modified the original thickness, and (3) the relatively low percentage of outcrop, preventing unambiguous assessment of the presence of second-order Alpine faults.

2.4 Case Tuberto-Calizzano unit: Alpine deformation and metamorphism

The Alpine deformation developed through several events [*Seno* et al., 2005a, b; *Bonini* et al., 2010; *Maino* et al., 2013], which are especially preserved in the sedimentary cover. The basement rocks record minor evidence of Alpine deformation, mostly represented by fracturing and fracture cleavage. The Meso-Cenozoic sedimentary succession shows two generation of folding and related cleavage [*Dallagiovanna*, 1988] (Fig. 4A-B) associated with a widespread network of quartz veins. Basement rocks rarely preserve evidence of an Alpine overprint, which is characterized by different paragenesis in the different lithologies. Peak conditions are indicated by the following mineral associations: chlorite+albite+pumpellyite in the gneisses, chlorite+albite+epidote in the amphibolites, chlorite+phengite+pumpellyite+albite±epidote (locally also lawsonite and Na-amphibole) in the Permian metavolcanites, chlorite+pumpellyite+albite±mica+quartz in the Triassic quartzites, sericite+chlorite in the Jurassic-Eocene pelites [*Messiga* et al*.,* 1981*; Cortesogno,* 1984*; Cortesogno* et al., 1998; *Desmons* et al., 1999a, 1999b; *Cortesogno* et al., 2002]. These mineral assemblages suggest a wide range of P-T re-equilibration conditions changing from prehnite-pumpellyite-, greenschist- to blueschist-facies conditions (pressure between 0.2-0.6 GPa and a temperature range between 250 and 400 °C), in distinct lithologies and/or in different structural positions. In fact, most of the relatively high P-T conditions assemblages are described in samples collected close to the main Alpine shear zone (e.g. Rio Nero, Case Volte). The highest temperatures were attained along major tectonic contacts, probably due to the effect of shear heating and/or fluid flow [*Maino et al.*, 2015]. However, the preservation of ^{40}Ar-^{39}Ar ages >274 Ma in white mica in analogous basement units (Savona and Nucetto massifs) [*Barbieri* et al., 2003] and one zircon fission track age of ~179 Ma [*Vance*, 1999] from the basement rocks suggests that the Alpine metamorphism probably did not exceed their relative closure temperatures (~350° C and ~240±25 °C, respectively) [*Reiners and Brandon*, 2006], thus questioning the effective temperature experienced by the Calizzano basement during the Alpine evolution. Because of the scarce Alpine relicts and the general lack of obvious relationships with the pre-Alpine associations and structures, it is not clear if these heterogeneous P-T conditions represent i) a single Alpine stage differently recorded by different rocks, ii) several Alpine stages; iii) several post-Variscan (i.e., not all Alpine) stages.

3 SAMPLE DESCRIPTION

Zircon fission track (ZFT) and (U-Th)/He (ZHe) analyses were carried out on 7 samples collected from the Calizzano-Case Tuberto unit with the aim of constraining the thermal path experienced by the basement during the rifting and subsequent collisional stages. The samples correspond to Late Cambrian-Lower Ordovician orthogneiss I (samples MB1403-06) and

Middle Ordovician orthogneiss II (MB1402, JT1014), which experienced pre-Variscan and/or Variscan (Early Ordovician and Carboniferous, respectively) amphibolite facies metamorphism [*Cortesogno*, 1984; *Gaggero* et al., 2004].

3.1 Field observations

In the sampling locations, the Variscan foliation in the orthogneisses is usually deformed and cut by distinct generations of mm- to cm-thick quartz veins (Fig. 4C). These veins generally cut the deformed pre-Alpine foliation and comprise pure quartz or alternatively quartz with sharp chlorite bands at the contact with the host rock (Fig. 4D). In addition, in selected localities this mineralization also affects the overlying sediments. Near Mereta and Calizzano villages (Fig. 3), a breccia formed by orthogneisses and minor carbonate clasts directly covers the basement (Fig. 4E). The clasts, from cm to m in size, are characterized by sharp rounded edges. The breccia is so pervasively silicified that the boundary with the orthogneiss clasts is completely masked (Fig. 4E). These features suggest a marked interaction with silicifying fluids circulating both inside the sampled basement rocks and in the overlying breccia.

3.2 Sample petrography

We present analyses of three types of granites:

(i) the first type (MB 1405 sample) is a two-mica gneiss characterized by Variscan foliation defined by white mica and brown biotite, both medium-grained and undeformed. An older generation of coarser-grained, deformed white mica and brown biotite is wrapped around by the main foliation or defines a former foliation (Fig. 5C). Medium-grained granoblastic quartz and poorly sericitized plagioclase are the other major rock-forming minerals. The textural and mineralogical features of this sample correspond to those of the paragneisses of the Gneiss-Amphibolite Complex [e.g., *Cortesogno*, 1984; *Gaggero* et al., 2004]. Fine-grained static recrystallization of white mica (Fig. 6A-B) and neoblastic growth of green biotite flakes (Fig. 6D-G), locally on former brown biotite (Fig. 6C), occur along micro-shear zones crosscutting the main foliation (Fig. 6A, B, C, E). The green biotite has higher FeO_{tot} contents (20.37-22.14 wt%) and both lower TiO_2 contents (1.13-1.75 wt%) and TiO_2/MgO ratio (0.11-0.17) with respect to the brown biotite (FeO_{tot} = 18.52-20.56 wt%; TiO_2 = 2.21-3.06 wt%; TiO_2/MgO = 0.23-0.35; Fig. 5 H and Table 2). Chlorite partly replaces both green and brown biotite (Fig. 6A, B, C, F, G).

(ii) The second type (MB1403-1404 1406 samples) is represented by a two mica augen-gneiss (Fig. 5D) in which granoblastic, poorly sericitized K-feldspar is in equilibrium with a Variscan foliation defined by quartz ribbons and medium-grained white mica and biotite. An older generation of coarse-grained white mica and biotite also occurs. The K-feldspar is characterized by a rim of plagioclase and myrmekites (Fig. 6E). These samples, which correspond to the Orthogneiss I of previous authors [e.g., *Gaggero* et al., 2004], do not show evidence for a late, greenschist-facies mineral assemblage.

(iii) The third type (JT1014, MB1402) is represented by a coarser-grained biotitic augen-gneiss (Fig. 5F) in which only one generation of Variscan biotite, defining the main foliation, is present. The K-feldspar porphyroclasts, poorly sericitized, show magmatic inclusions of lobate quartz and subhedral biotite. In the studied samples, the local growth of white mica + chlorite partly replaces the former brown biotite. The lack of polyphase deformation and the relict magmatic microstructures indicate that these samples correspond to the Orthogneiss II of previous authors [e.g., *Gaggero* et al., 2004].

4 METHODS

4.1 Biotite chemical composition

Compositions of brown and green biotite in sample MB 1405 were obtained with a JEOL JSM IT300LV (High Vacuum – Low Vacuum 10/650 Pa - 0.3-30kV) SEM equipped with an EDS Oxford INCA Energy 200 with detector INCA X-act SDD thin window at the Department of Earth Sciences, University of Torino. The operating conditions were as follows: 30 s counting time and 15 kV accelerating voltage. The quantitative data (spot size = 2 μm) were acquired and processed using the Microanalysis Suite Issue 12, INCA Suite version 4.01; natural mineral standards were used to calibrate the raw data; the ρφZ correction (*Pouchou and Pichoir*, 1988) was applied. Absolute error is 1 σ for all calculated oxides.

4.2 Zircon Fission Track dating

Zircon separates were mounted into Teflon pads, which were polished to expose internal surfaces. Two to three mounts per sample were prepared according to the availability of zircons in order to adopt the multiple-etch technique of *Naeser* et al. [1987]. The mounts were etched in a eutectic melt of NaOH and KOH at 228 ºC for either 7, 14 or 28 hr. Mica laminae were attached to the samples as external detectors. The mounts were then irradiated at the Radiation Center of Oregon State University, using a nominal Neutron fluence of $1*10^{15}$ ncm^{-2}. Induced tracks were revealed by etching in 40% HF at 21°C for 45 min. Fission tracks were analysed on all the countable grains from the 7 and 14 hr etches, while the long etch resulted in over-etched samples. The Fish Canyon tuff was used as a standard for the zeta calibration

[*Hurford and Green*, 1983]. The age distribution of the pooled ages of all samples were decomposed into dominant age peaks using the BinomFit program of *Brandon* [2002], version 1.2.63 (2007).

4.3 Zircon (U-Th)/He dating

Zircon crystals were selected on the basis of size, morphology and absence of inclusions. Crystals with two pyramidal terminations and undamaged surfaces were handpicked and their dimensions measured. From each sample, one crystal was individually loaded into Pt-foil capsules. The average crystal widths ranged from 39.4 to 71 μm. Most of the selected grains have small radii because larger crystals are mostly affected by intense fracturing and/or presence of inclusions.

(U-Th)/He age determinations were performed at the Scottish Universities Environmental Research Centre. Complete Helium extraction was achieved by heating the Pt foils using an 808 nm diode laser for 20 minutes at 1100-1300°C. ^{4}He concentrations were measured by peak height comparison to a calibrated standard using a Hiden HAL3F quadrupole mass spectrometer, following the protocols of *Foeken et al.* [2006]. All samples were reheated two or three times to ensure complete degassing. U and Th determinations were made after extraction of the crystals from the Pt foil. The degassed zircons were spiked with a known amount of ^{235}U and ^{230}Th and dissolved in a Parr™ bomb acid digestion vessel. Ion exchange column chemistry was used to remove the Pt and other matrix elements. U and Th were measured on a VG PlasmaQuad-2 ICPMS. The calculated ages (‘raw ages’) have been corrected to account for He loss because of α-recoil [Ft; *Farley et al.*, 1996] following the method of *Ketcham et al.* [2011]. The uncertainty associated with the Ft correction factor calculation is propagated into the total uncertainty of the Ft-corrected (U-Th)/He ages.

An uncertainty of 11.9% (2σ) is assumed for individual age determination (Table 2), based on the age reproducibility of the Fish Canyon Tuff ZHe age standard [*Dobson et al.*, 2008]. The 2σ age reproducibility of each sample was also calculated. Apart from sample MB1406, all other samples have age reproducibility comparable to the zircon age standard. In order to constrain the time–temperature (t–T) history of selected samples, inverse modelling of the ZHe ages was performed using HeFTy [*Ketcham*, 2005]. We have exploited the dependence of the He closure temperature (Tc) on grain size, cooling rate and eU content [*Reiners*, 2005].

5 RESULTS

5.1 Zircon fission track data

Details of the sample ages and the age populations are reported in Table 1. All the count data and the radial plots are provided in the auxiliary material. The age distribution and the central age of each sample is plotted in Figure 7. Six samples provided enough zircons for fission-track dating. Among these six samples, the amount of countable zircons is highly variable, from 18 to 60 grains per sample. The resulting central ages range from 138.1 to 168.6 Ma and average to 156.2 Ma with a standard deviation of 7%. The analytical error (1σ) of the central ages vary between 6% (MB1406) and 9% (MB1402) and 5 out 6 samples overlap within this error with the exception of sample mb1405, which is significantly younger than most samples (147.5±9.0 Ma, Fig 7) only if the 1σ error or the 68% confidential intervals are considered. Two samples (MB 1402-1404) have a probability χ^2 value lower than 5% that indicates larger than expected Poissonian scatter in track count data. Thus, these two samples could consist of multiple age populations, whereas all the other samples consist of single age populations. An extra Poissonian age scatter is often observed for zircon fission-track age distribution even in samples that are expected to have a single age population [e.g. *Fellin et al.,* 2006]. Such scatter can be partly attributed to the wide range in U concentrations typical of zircons, resulting in highly variable degree of radiation damage, which together with temperature controls the annealing of tracks. The number of countable grains in the two highly scattered samples is too low (19 and 38 grains) to derive statistically their age components. Their central and pooled ages have a difference of < 1 Ma which also indicate that multiple age populations cannot be resolved within these two samples. Thus, although different age populations cannot be resolved within individual samples, they could be resolved by pooling the grains together from all samples. The pooled grains amount to 196 and their distribution is formed by 3 age components (Fig. 8). The largest population, formed by 71% of the grains, is centered at 156.2 Ma, which is exactly the same as the average of all the central ages of the samples. The other 2 populations are centered at 128.7 and 214.9 Ma and are formed by 21% and 7% of the grains, respectively. Thus, the average of the central ages of the samples and the main population of the pooled ages all consistently indicate a major age component at ~150-160 Ma. The young population at 128.7 Ma could relate to partial rejuvenation related to the Alpine overprint. The oldest population at 214.9 Ma could relate to zircons that are most resistant to annealing.

5.2 Zircon (U-Th)/He data

Twelve ZHe age determinations performed on six samples (Table 2; Fig. 7) supplied five pairs of ages with reproducibility within the individual uncertainty (2σ). Reproducing ages range from 78 ± 9.3 to 6.9 ± 0.8 Ma. Sample MB1406 shows two very different ages (10.3 and 52.8 Ma) indicating poor reproducibility. Samples MB1404 and MB1405 are between 28.3 ± 3.3 and 29.4 ± 3.5 Ma, accordingly with the Oligocene Alpine ZHe ages reported from the other units of the Ligurian Alps [*Maino et al.*, 2012a; 2015]. Samples MB1403 and

JT1014 show younger ages (between 6.9 ± 0.8 and 12.6 ± 1.5 Ma) close to the AFT data reported in the study area [*Foeken et al*., 2003]. Only the sample MB1402, collected close to the basement-cover boundary (Fig. 2), has an old, pre-Alpine age of 78 ± 9.3 Ma. Noticeably, this sample has the largest mean crystal radii (61.5-71 μm), suggesting a positive correlation between grain size and age. The considerably different ages from samples without relevant differences of elevation or structural position can be ascribed to many factors influencing the sensitivity of the (U-Th)/He system, including radiation damage [*Flowers et al.*, 2007; *Guenthner et al.*, 2013], the accuracy of the Ft correction [*Reiners et al.*, 2011], U and Th zonation [*Dobson et al.,* 2008] and the residence time of zircons within the partial retention zone (150-220 °C) [*Reiners et al.,* 2004; *Guenthner et al.*, 2013]. These factors can influence the results particularly for zircons that experienced a complex geological history as in our case. In particular, a high radiation damage accumulation is suggested by the negative date-effective uranium (eU) correlation [*Guenthner et al.*, 2013] derived from the analyzed zircons (Fig. 9A). Furthermore, the ZHe ages show a strong positive correlation with the grain sizes (Fig. 9B), where the largest crystals were not reset, thus suggesting that the zircons experienced temperatures close to the lower boundary of the partial retention zone.

6 DISCUSSION

ZFT single-grain ages from the Case Tuberto-Calizzano unit span a large age range from 340 to 83 Ma. These ages fill the gap between the Rb/Sr and $^{40}Ar/^{39}Ar$ ages (327-274 Ma in the Briançonnais-Prepiedmont units; [*Del Moro et al.*, 1982a; *Barbieri et al.*, 2003]) and the ZHe ages (78-7 Ma, this study and *Maino et al*. [2012a]).

The large ZFT age range can be partly related simply to the Poissonian age scatter typical of fission-track data but it could also reflect a long residence time of the studied rocks in the ZFT partial annealing zone that would result in a wide annealing degree. The consistency among the central ages, and between those ages and the age of the largest population (71%) of the pooled grains, indicate that cooling below the ZFT closure temperature (~240º C, [*Brandon et al.*, 1998]) likely occurred at around 150-160 Ma. The dependency between closure temperature and cooling rate and the general shortage of constraints available on the thermal history of the studied rocks make it difficult to derive the temperature at which closure of our ZFT ages occurred. In fact, for cooling rates in the order of 10 ºC/km, the closure temperature is ~240 ºC (Reiners and Brandon, 2006) but for slow cooling of 0.6 ºC/Myr it is as low as 205 ºC (Bernet, 2008). Nevertheless, the timing of cooling as constrained by our ZFT data indicates that the Jurassic rifting is a possible reason for the heating/cooling cycle. The lower ZFT annealing zone overlaps with the upper ZHe retention zone at temperatures higher than ~180º C such that the temperatures required to attain incomplete reset of the ZHe ages may cause partial rejuvenation of the most sensitive zircons and therefore may explain some of the youngest ZFT ages observed in our samples.

Tertiary ages for the Alpine metamorphism are heterogeneously recorded by the ZHe ages, suggesting partial to total resetting. While the ages between 29 and 7 Ma fit with the Alpine regional cooling ages [*Foeken et al.*, 2003; *Maino et al.*, 2012a], the age between 78 and 53 Ma are considerably older. This wide variation is probably due to high radiation damage accumulation, as indicated by the negative date-effective uranium (eU) correlation and the positive grain size/age correlation (Fig. 9A, B; Table 2). The ZHe age thermal model corroborates that the Alpine tectono-metamorphic phases were attained in a short interval at low-T condition (Fig. 9C), not sufficient to completely reset the ZHe ages (i.e. temperatures were around 180°C for a few Myr).

However, mineral parageneses indicate Alpine metamorphism at T ~250-400 °C. Such temperatures are considerably higher than those required to completely reset both ZHe and ZFT ages. Therefore, an apparent discrepancy exists between the constraints derived from the metamorphic assemblages and those based on the degree of resetting of the thermochronometric ages. In order to reconcile the different lines of evidence, we should consider - as first point - the distribution of the Alpine metamorphic record, which is locally recorded mostly along shear zones, it does not pervade the rocks and it is characterized by highly variable paragenesis in different lithologies and locations [Messiga et al., 1981]. Most of the Calizzano and Case Tuberto rocks show evidence of low-T (prehnite-pumpellyite facies) Alpine metamorphism and deformation (fracturing and fracture cleavage). Indeed, the higher P-T paragenesis (greenschist-to-blueschist facies) have been found mostly along Alpine shear zones, suggesting the possible influence of local heating (and pressure increase) associated with focused deformation [e.g. Maino et al., 2015]. This suggests that, far from sites of high strain where higher P-T conditions were attained, the Alpine metamorphism may have developed as a low-T thermal pulse.

A second possible explanation for the discrepancy between metamorphic and thermochronometric record is that part of the paragenesis previously ascribed to the Alpine stage were developed during a pre-Alpine (but post-Variscan) thermal event. In the study area, the Variscan cycle ends with a greenschist-facies folding event developing actinolite+chlorite along axial planes [*Gaggero* et al., 2004]. In lithologies with suitable bulk composition, the growth of green biotite along micro-shear zones crosscutting Variscan microstructures, and its partial replacement by Alpine chlorite along fractures (Fig. 6), records a tectono-metamorphic event that occurred between the Variscan and Alpine orogeneses. It is known that a systematic change in biotite color from greenish-brown to reddish-brown/black occurs with increasing metamorphism and is due to variations in chemical composition (*Engel and Engel*, 1960). In particular, the greenish color is produced by high Fe_{tot} coupled with low TiO_2/MgO ratio (Fig. 5H) and it is indicative of low metamorphic grade (Engel & Engel, 1960; Henry et al., 2005). In fact, in suitable lithologies, the formation of prograde green biotite at low metamorphic grade can occur as a result of reactions involving K-feldspar and chlorite [*Verschure et al.,* 1980] and its presence can be taken as indicative of temperatures around 350–450°C [*Jäger*, 1967; *Verschure et al.*, 1980; *Del Moro et al.*, 1982b; *Satır & Friedrichsen*, 1986; *Blanckenburg et al.*, 1989; *Bozkurt et al.* 2011]. Thus, the green biotite indicates that the studied area experienced a post-Variscan, pre-Alpine heating event at HT greenschist-facies conditions during the extensional regime. A similar event is also recorded in phyllonites containing green biotite, formed along a Jurassic detachment in the distal margin represented by the Canavese Zone (Western Alps; *Ferrando et al.* 2004).

We infer that, in the study area, an anomalously high geothermal gradient coupled with a pervasive circulation of hot fluids were responsible for the quartz mineralization (Fig. 4) and for the growth of green biotite in suitable lithologies (Fig. 6).

Such conditions could be met in an extended rift system where heating/cooling cycles are typically coupled with focused thinning, high geothermal gradients (~60-90°C/km; [*Liao et al*., 2014; *Vacherat et al*., 2014; *Hart et al., in press*]) and circulation of hot fluids. Moreover, these thermal conditions could explain the growth of the less diagnostic assemblage chlorite ± white mica in other lithologies of the study area. Our ZFT ages support this interpretation as they indicate that temperatures above ~200 Cº must have extensively affected the study area before 150-160 Ma. Thus, we suggest that at least part of the Alpine greenschist facies mineral assemblage reported by the previous studies in the Calizzano basement rocks [*Messiga et al*., 1981; *Cortesogno et al*., 1998] needs to be explained by invoking heating mechanisms other than the Alpine metamorphism and may be linked, instead, to Tethys rifting. An accurate estimate of the Jurassic burial depth of the sampled basement is difficult given the poor preservation of the syn-rift sedimentary record. Regardless, the sampled basement was probably located at shallow depth during rifting as we estimate that our most superficial basement samples were probably at less than 2-3 km below syn-rift sediments.

Assuming a surface temperature between 10 and 20°C and a geothermal gradient of 80°C/km, typical of hyperextended margins [*Vacherat et al*., 2014; *Hart et al.,* 2017], this depth corresponds to temperatures between ~170 and 260°C, which are in the range of the ZFT partial annealing zone (~200-260°C; [Reiners and Brandon, 2006]). Furthermore, circulating fluids, possibly within crustal fault systems, may have affected heat transfer at such shallow crustal levels. A similar mechanism was proposed by *Beltrando et al.* [2015] to explain the cooling ages of the distal margin exposed in the Southalpine domain of the Alps.

To decipher the significance of the above-described scenario in the Case Tuberto-Calizzano unit at the scale of the European rifted margin, the palaeo-structural location within an Alpine rift of this nappe must be considered (Fig. 10). In the section proposed by *Decarlis* et al. [2015] across the European margin exposed in Liguria, the Case Tuberto-Calizzano unit is located at the boundary between the Briançonnais and Prepiedmont domains [see *Vanossi*, 1991; *Decarlis et al*. 2013]. This domain was characterized by one of the major fault systems that accommodated crustal thinning within the future distal margin (i.e. φ fault in Fig. 10). This fault system controlled the development of the distal margin juxtaposing the elevated and uplifted Briançonnais block [*Decarlis and Lualdi*, 2008] against the delaminated and strongly subsiding Prepiedmont domain [*Decarlis and Lualdi*, 2010] during the late Early Jurassic. During the Middle Jurassic, the emerged sector of the distal margin drowned, as testified by the renewal of deposition atop [*Decarlis and Lualdi*, 2008; *Decarlis* et al., 2013], and deformation migrated towards the future ocean along a detachment system initiating active exhumation (ε fault in Fig. 10)

In a rift model such as that shown in Figure 10, the Case Tuberto-Calizzano unit might have been passively affected by a heating event induced by the combined action of crustal/lithospheric thinning and the activation of hydrothermal systems along brittle faults (φ-like). Fault systems might have played a first-order role in transporting heat toward the surface through remobilization of deep-seated fluid circulation during the final stages of rifting (i.e. during the thinning phase: Pliensbachian-Toarcian). Subsequent tectonic quiescence of the fault system during the Middle Jurassic, due to lithospheric onset of exhumation led to the progressive cooling of the distal margin that is recorded by the ZFT data. A similar timing for active hydrothermal fluid systems associated with Jurassic rifting in the distal Alpine Tethys margin has been recently proposed by *Incerpi et al*. [2017].

Thus, both the present study and the literature data suggest that relatively high temperatures (between ~200 and 400°C) might have been acquired during crustal/lithospheric thinning driven by fluid activity in the upper crust at different locations along the Alpine Tethys distal margins [e.g. *Beltrando et al*. 2015, *Incerpi et al*. 2017]. Our study demonstrates that such conditions were able to generate metamorphic paragenesis (greenschist facies) at very shallow crustal levels of < 2-3 km. The temperature peak was reached during the formation of the future distal margin and cooling initiated at the onset of exhumation and migration of active tectonics further oceanwards.

7 CONCLUSIONS

Thermochronometric analysis of basement rocks belonging to the Case Tuberto-Calizzano unit led to the recognition of two distinct heating-cooling cycles that have been respectively attributed to the Alpine Tethys rifting stage (ZFT ages of ~150-160 Ma) and to the Alpine orogenic deformation (ZHe ages of ~29.4 to 7 Ma). These data coupled with the local growth of green biotite (stable at about 350-450°C) in lithologies with suitable bulk composition and evidence for abundant mineralization, suggest that the temperatures reached during the rifting stage exceeded those of the Alpine metamorphism in the study area. The incomplete reset of the ZHe ages and the non-reset of the ZFT ages during the Alpine metamorphism indicate that the well documented Alpine deformation had to occur under conditions from prehnite-pumpellyte to low temperature blueschists facies at temperatures lower than ~200 ºC. Thus, the Alpine metamorphic overprint must have occurred during a short-lived low temperature pulse. The lack of pervasive Alpine resetting of the ages allowed the preservation of an older heating-cooling event that occurred during Alpine Tethys rifting. Considering the peculiar position of the study area in the former Jurassic rifted margin, heating may have been caused by the combined effect of severe crustal/lithospheric thinning in the distal domain associated with high geothermal gradients and hydrothermal circulation along brittle faults. This latter might have focused hot deep-seated fluids towards shallow crustal levels, which are represented by the studied Case Tuberto-Calizzano unit (samples located at less than 2-3 km depth during rifting), causing basement heating during the thinning phase (Pliensbachian-Toarcian) with a similar mechanism to that suggested by *Beltrando et al.* [2015]. The following stages of rifting, i.e. the beginning of exhumation in the more distal parts of the distal margin, resulted in a tectonic quiescence (probably since the Bajocian-Bathonian) and progressive cooling of the basement that was recorded by the Middle Jurassic ZFT ages and completed during the Late Jurassic. The rift-related heating, often difficult to recognize in mountain belts due to the orogenic overprint, can be recognized in the Case Tuberto-Calizzano unit. Therefore, this latter unit can be considered as an excellent “fossil analogue” within which future research may qualitatively and qualitatively estimate the thermal evolution and heat transfer mechanisms occurring at distal magma-poor rifted margins during final rifting and plate separation.

ACKNOWLEDGEMENTS

We gratefully thank Philip Ball, Virginia Toy and two anonymous reviewers for helpful reviews that significantly improve the manuscript. The research was supported by Torino University Grant (Torino_call2014_L1_202; Resp. S.F.) and by MM4 consortium (Margin Modelling Phase 4: Liverpool & Strasbourg University), taking benefits from useful discussions with colleagues from the academic and industrial partners. The data supporting this paper are available within tables, figures and supplemental material section.

REFERENCE

Airoldi, M. (1937), Rilevamenti geologici nelle Alpi Liguri. II. Il Massiccio di Calizzano, *Bollettino della Società Geologica Italiana*, 56, 467-498.

Barbieri, C., B. Carrapa , A. Di Giulio, J. Wijbrans and G. Murrell (2003), Provenance of Oligocene synorogenic sediments of the Ligurian Alps (NW Italy): Inferences on belt age and cooling history, *Int. J. Earth Sci.*, 92, 758–778.

Beltrando M., D. F. Stockli, A. Decarlis and G. Manatschal (2015), A crustal-scale view at rift localization along the fossil Adriatic margin of the Alpine Tethys preserved in NW Italy, *Tectonics*, 34, 1927-1951, doi: 10.1002/2015TC003973.

Blanckenburg, V.F., I. M. Villa, H. Baur, G. Morteani, R. H. Steiger (1989), Time calibration of a PT-path from the Western Tauern Window, Eastern Alps: the problem of closure temperatures. *Contributions to Mineralogy and Petrology*, 101, 1–11.

Bonini, L., G. Dallagiovanna and S. Seno (2010), The role of pre-existing faults in the structural evolution of thrust systems: insights from the Ligurian Alps (Italy), *Tectonophysics*, 480, 73–87.

Bozkurt, E., et al. (2011), Surprisingly young Rb/Sr ages from the Simav extensional detachment fault zone, northern Menderes Massif, Turkey., *Journal of Geodynamics*, *52*, 406-431.

Brandon, M. T. (2002), Decomposition of mixed grain age distributions using BINOMFIT, *On Track*, 24, 1–18.

Capponi, G. and L. Crispini (2002), Structural and metamorphic signature of alpine tectonics in the Voltri Massif (Ligurian Alps, North-Western Italy), *Eclogae Geologicae Helvetiae,* 95, 31–42.

Claudel, M. E. and T. Dumont (1999), A record of multistage continental break-up on the Briançonnais marginal plateau (Western Alps): Early and Middle Jurassic rifting, *Eclogae Geologicae Helvetiae*, 92, 45–61.

Cortesogno, L. (1984), Metamorfismo e magmatismo prealpini nel basamento e nel tegumento delle Alpi Liguri. *Memorie della Società Geologica Italiana*, 28, 79-94.

Cortesogno, L., G. Dallagiovanna, L. Gaggero and M. Vanossi (1993), Elements of the Palaeozoic History of the Ligurian Alps. In: von Raumer, J.F., Neubauer, F. Eds. , Pre-Mesozoic Geology in the Alps. Springer-Verlag, pp. 257–277.

Cortesogno, L., G. Dallagiovanna, L. Gaggero , S. Seno and M. Vanossi (1998), Tettonica vulcanismo tardo-Paleozoici nel dominio prepiemontese delle Alpi Liguri: la testimonianza della successione del Colle Scravaion. *Atti Ticinesi Scienze della Terra*, s.s. 7, 17-26.

Cortesogno, L., L. Gaggero, G. Lucchetti and R. Cabella (2002), Compositions and miscibility gap in Na-Ca clinopyroxenes through high-pressure metamorphism. Per. Mineral., 71/1, 1-25.

Crozi, M. (1998), Basamento e coperture prepiemontesi tra il colle di San Bernardo ed il colle Scravaion (alpi Liguri): precisazioni stratigrafiche e strutturali, M.S. thesis, Dep. of Earth Sciences, Univ. Of Pavia, Italy

Dallagiovanna, G. (1988), Testimonianze e significato di una trasgressione permo-triassica sul basamento cristallino del Brianzonese Ligure Interno, *Bollettino della società Geologica Italiana*, 107, 445-451.

Dallagiovanna, G. and S. Seno (1984), Rilevamento geologico ed analisi strutturale del settore meridionale dell'unita` di Arnasco-Castelbianco (Alpi Marittime), *Memorie della Società Geologica Italiana*, 28, 441–445

Dallagiovanna, G., A. Lualdi, S. Seno and M. Vanossi (1984), Nuovi dati e precisazioni sull'Unità di C. Tuberto (Prepiemontese delle Alpi Liguri), *Memorie della Società Geologica Italiana*, 28, 419-430.

Dallagiovanna, G., L. Gaggero, M. Maino, S. Seno and M. Tiepolo (2009), U–Pb zircon ages for post-Variscan volcanism in the Ligurian Alps (Northern Italy), J. Geol. Soc., 166, 1–14. doi: 10.1144/0016-76492008-027

Decarlis, A. and A. Lualdi (2008), Late Triassic-Early Jurassic paleokarst from the Ligurian Alps and its geological significance (Siderolitico Auct., Ligurian Briançonnais domain), *Swiss Journal of Geosciences*, 101, 579–593.

Decarlis, A. and A. Lualdi (2011), Synrift sedimentation on the northern Tethys margin: an example from the Ligurian Alps (Upper Triassic to Lower Cretaceous, Prepiedmont domain, Italy), *International Journal of Earth Sciences,* 100, 1589–1604.

Decarlis, A., G. Dallagiovanna, A. Lualdi, M. Maino and S. Seno (2013), Stratigraphic evolution in the Ligurian Alps between Variscan heritages and the Alpine Tethys opening: a review, *Earth Science Reviews*, 125, 43-68. doi:10.1016/j.earscirev.2013.07.001.

Decarlis, A., M. Maino, G. Dallagiovanna, A. Lualdi, E. Masini, G. Toscani and S. Seno (2014), Salt tectonics in the SW Alps (Italy–France): From rifting to the inversion of the European continental margin in a context of oblique convergence, *Tectonophysics*, 636, p. 293–314, doi:10.1016/j.tecto.2014.09.003.

Decarlis, A., G. Manatschal, I. Haupert and E. Masini (2015), The tectono-stratigraphic evolution of distal, hyper-extended magma-poor conjugate rifted margins: Examples from the Alpine Tethys and Newfoundland Iberia, *Marine and Petroleum Geology*, 68, 54-72.

Decarlis A., M. Beltrando, G. Manatschal, S. Ferrando and R. Carosi (in press), Architecture of the distal Piedmont-Ligurian rifted margin in NW-Italy: hints for a flip of the rift system polarity, Tectonics, Doi: 10.1002/2017TC004561.

De Graciansky, P. C., D. G. Roberts and P. Tricart (2011), The Western Alps, from rift to passive margin to orogenic belt: an integrated geoscience overview, *Developments in Earth Surface Processes*, 14, Elsevier: 397 pp, doi: https://doi.org/10.1016/c2009-0-64485-8

Del Moro, A., G. Pardini, B. Messiga and M. Poggio (1982a), Dati petrologici e radiometrici preliminari sui massicci cristalllini della Liguria Occidentale, *Rendiconti della Società Italiana di Mineralogia e Petrografia*, 38 (1), 73-87.

Del Moro, A., M. Puxeddu, F. Radicati di Brozolo and I. M. Villa (1982b), Rb-Sr and K-Ar ages on minerals at temperatures of 300–400 °C from deep wells in the Larderello geothermal field (Italy). *Contributions to Mineralogy and Petrology*, 81, 340–349.

Desmons, J., R. Compagnoni, L. Cortesogno, M. Frey, L. Gaggero (1999a), Pre-Alpine metamorphism of the Internal zones of the Western Alps. *Schweizerische Mineralogische und Petrographische Mitteilungen*, 79, 23-39.

Desmons J., J. Aprahamian, R. Compagnoni, L. Cortesogno, M. Frey, L. Gaggero, G. Dallagiovanna and S. Seno (1999b), Alpine metamorphism of the Western Alps: I. Middle to high T/P metamorphism, *Schweizerische Mineralogische und Petrographische Mitteilungen* 79, 89-110.

Dobson, K. J., F. M. Stuart, T. J. Dempster and EIMF (2008), U and Th zonation in Fish Canyon Tuff zircons: Implications for a zircon (U-Th)/He standard: *Geochimica Cosmochimica Acta*, 72, 4745-4755.

Engel, A.E.J. and C. Engel (1960), Progressive metamorphism and granitization of the major paragneiss, northwest Adirondack Mountains, New York: mineralogy, *Geological Society of America Bulletin*, 71, 1-58.

Farley, K. A., R. A. Wolf and L. T. Silver (1996), The effects of long alpha-stopping distances on (U-Th)/He ages, *Geochimica et Cosmochimica Acta*, 60, 4223-4229.

Fellin, M.G., J. Vance , J. I. Garver and M. Zattin (2006), The thermal evolution of Corsica as recorded by zircon fission-tracks, *Tectonophysics,* 421, 299-317.

Ferrando, S., D. Bernoulli and R. Compagnoni (2004), The Canavese zone (internal western Alps), a distal margin of Adria. *Schweizerische Mineralogische und Petrographische Mitteilungen*, 84, 1-20.

Flowers, R. M., D. L. Shuster, B. P. Wernicke and K. A. Farley (2007), Radiation damage control on apatite (U–Th)/He dates from the Grand Canyon region, Colorado Plateau, *Geology*, 35, 447–450.

Foeken, J. P. T., T. J. Dunai, G. Bertotti and P. A. M. Andriessen (2003), Late Miocene to present exhumation in the Ligurian Alps (southwest Alps) with evidence for accelerated denudation during the Messinian salinity crisis, *Geology*, 31, 797–800.

Foeken, J. P. T., F. M. Stuart, K. J. Dobson C. Persano and D. Vilbert (2006), A diode laser systemfor heating minerals for (U-Th)/He chronometry: *Geochemistry Geophysics Geosystems*, 7, Q04015, doi:10.1029/2005GC001190.

Froitzheim, N. and G. Manatschal (1996), Kinematics of Jurassic rifting, mantle exhumation, and passive-margin in the Austroalpine and Penninic nappes (eastern Switzerland), *Geol. Soc. of Am. Bull.*, 108, 1120–1133.

Gaggero, L., L. Cortesogno and J. M. Bertrand (2004), The Pre-Namurian basement of the Ligurian Alps: a review of the lithostratigraphy, pre-Alpine metamorphic evolution and regional comparisons, *Periodico di Mineralogia*, 73, 85-96.

Guenthner, W. R., P. W. Reiners, R. A. Ketcham, L. Nasdala and G. Giester (2013), Helium Diffusion in Natural Zircon: Radiation Damage, Anisotropy and the interpretation of zircon (U-Th)/He Thermochronology, *Am. J. Sci*. 313, 145–198.

Hart, N. R., D. F. Stockli, L. L. Lavier and N. W. Hayman (in press), Thermal Evolution of a hyperextended rift basin, Mauleon Basin, western Pyrenees, Tectonics, doi: 10.1002/2016TC004365.

Haupert, I., G. Manatschal, A. Decarlis and P. Unternehr (2016), Upper-plate magma-poor rifted margins: Stratigraphic architecture and structural evolution, *Marine and Petroleum Geology*, 69, p. 241-261.

Henry, D. J., et al. (2005), The Ti-saturation surface for low-to-medium pressure metapelitic biotites: implications for geothermometry and Ti-substitution mechanisms., *American Mineralogist, 90,* 316-328.

Hurford, A.J. and P. F. Green (1983), The Zeta calibration of fission track dating, *Chemical Geology*, 41, 285-317.

Incerpi, N., L. Martire, G. Manatschal and S. M. Bernasconi (2017) Evidence of hydrothermal fluid flow in a hyperextended rifted margin: the case study of the Err Nappe (SE Switzerland), *Swiss Journal of Geoscience*, DOI: 10.1007/s00015-016-0235-2.

Jäger, E. (1967), Die Bedeutung der Biotit Alterswerte. In: Jäger E., Niggli E., Wenk E. (Eds.), Rb/Sr Altersbestimmungen an Glimmern der Zentralalpen. *Beitraege zur Geologischen Karte der Schweiz*, 66, pp. 28–31.

Ketcham, R. A., C. Gautheron and L. Tassan-Got (2011), Accounting for long alpha-particle stopping distances in (U–Th–Sm)/He geochronology: refinement of the baseline case. *Geochimica et Cosmochimica Acta*, 75(24), 7779-7791.

Lemoine, M. and R. Trümpy (1987), Pre-oceanic rifting in the Alps, *Tectonophysics*, 133, 305-320.

Liao, W. Z., Lin, A. T., Liu, C. S., Oung, J. N., and Y. Wang, (2014), Heat flow in the rifted continental margin of the South China Sea near Taiwan and its tectonic implications, *Journal of Asian Earth Sciences*, 92, 233-244.

Maino, M., G. Dallagiovanna, K. Dobson, L. Gaggero, C. Persano, S. Seno and F. M. Stuart (2012a), Testing models of orogen exhumation using zircon (U–Th)/He thermochronology: Insights from the Ligurian Alps, Northern Italy, *Tectonophysics*, 560/561, 84-93, 84–93, doi:10.1016/j.tecto.2012.06.045.

Maino, M., G. Dallagiovanna, L. Gaggero, S. Seno and M. Tiepolo (2012b), U–Pb zircon geochronological and petrographic constraints on late to post - collisional Variscan magmatism and metamorphism in the Ligurian Alps, Italy, *Geological Journal*, 47(6), 632-652. doi: 10.1002/gj.2421

Maino, M., A. Decarlis, F. Felletti and S. Seno (2013), Tectono-sedimentary evolution of the Tertiary Piedmont Basin (NW Italy) within the Oligo–Miocene central Mediterranean geodynamics, *Tectonics*, 32, 593-619, doi:10.1002/tect.20047.

Maino, M., L. Casini, A. Ceriani, A. Decarlis, A. Di Giulio, S. Seno, M. Setti and F. M. Stuart (2015), Dating shallow thrusts with zircon (U-Th)/He thermochronometry-The shear heating connection: *Geology*, 43/6, 495-498. doi: 10.1130/G36492.1

Manatschal, G. (2004), New models for evolution of magma-poor rifted margins based on a review of data and concepts from West Iberia and the Alps. *International Journal of Earth Science*, 93, 432–466.

Manatschal, G. and D. Bernoulli (1999), Architecture and tectonic evolution of non-volcanic margins: present-day Galicia and ancient Adria, *Tectonics*, 18(6), 1099-1199.

Masini, E., G., Manatschal and G. Mohn (2013), The Alpine Tethys rifted margins: reconciling old and new ideas to understand the stratigraphic architecture of magma-poor rifted margins, Sedimentology, 60, 174-196.

Messiga B., M. Oxilia, G. B. Piccardo and M. Vanossi (1981), Fasi metamorfiche e deformazioni Alpine nel Brianzonese e nel Pre-Piemontese – Piemontese esterno delle Alpi Liguri: un possible modello evolutivo, *Rendiconti della Società Italiana di Mineralogia e Petrologia*, 38(1), 261-280.

Mohn G., G. Manatschal, M. Beltrando, E. Masini and N. Kusznir (2012), Necking of continental crust in magma-poor rifted margins: Evidence from the fossil Alpine Tethys margins: *Tectonics*, 31, doi:10.1029/2011TC002961.

Naeser, N.D., P. K. Zeitler, C. W. Naeser and P. F. Cerveny (1987), Provenance studies by fission track dating of zircon–Etching and counting procedures, *Nuclear Tracks Radiation Measurements* 13, 121-126.

Pouchou, J.L. and F. Pichoir (1988), Determination of mass absorption coefficients for soft X-rays by use of the electron microprobe. Microbeam Analysis. San Francisco Press, San Francisco, 319–324 pp.

Reiners, P. W., T. L. Spell, S. Nicolescu and K. A. Zanetti (2004), Zircon (U-Th)/He thermochronometry: He diffusion and comparisons, *Cosmochim. Acta*, 68, 1857– 1887.

Reiners, P. W. and M. T. Brandon (2006), Using thermochronology to understand orogenic erosion, *Ann. Rev. Earth Planet. Sci.*, 34, 419–466.

Satır, M., H. Friedrichsen (1986), The origin and evolution of the Menderes Massif, WTurkey: a rubidium/strontium and oxygen isotope study, *Geologie Rundschau*, 75, 703–714.

Seno, S., G. Dallagiovanna and M. Vanossi (2005a), A kinematic evolution model for the Penninic sector of the central Ligurian Alps, *International Journal Earth Science*, 94, 114–129.

Seno, S., G. Dallagiovanna and M. Vanossi (2005b), Pre-Piedmont and Piedmont-Ligurian nappes in the central sector of the Ligurian Alps: A possible pathway for their superposition on to the inner Briançonnais units, *Bollettino Società Geologica Italiana*, 124(2), 455–464.

Seymour, N. M., D. F. Stockli, M. Beltrando and A. J. Smye (2016), Tracing the thermal evolution of the Corsican lower crust during Tethyan rifting. *Tectonics* 35, 2439–2466.

Sutra, E. , G. Manatschal, G. Mohn and P. Unternehr (2013), Quantification and restoration of extensional deformation along the Western Iberia and Newfoundland rifted margins. *Geoch., Geoph., Geosys*, 14 (8), 2575-2597.

Tugend, J., G. Manatschal, N. J. Kusznir and E. Masini (2014), Characterizing and identifying structural domains at rifted continental margins: application to the Bay of Biscay margins and its Western Pyrenean fossil remnants. *Geological Society of London*, S. P. 413.

Vacherat, A., F. Mouthereau, R. Pik, M. Bernet, C. Gautheron,, E. Masini, L. Le Pourhiet, B. Tibari and A. Lahfid (2014), Thermal imprint of rift-related processes in orogens as recorded in the Pyrenees. Earth and Planetary Science Letters, 408, 296-306.

Vance, J. (1999), Zircon fission track evidence for a Jurassic (Tethyan) thermal event in the Western Alps, *Memorie di Scienze Geologiche dell'Università di Padova*, 51, 473-476.

Vanossi, M. (Ed.) (1991), Guide Geologiche Regionali, Alpi Liguri. Be-Ma, Milan, 296 pp.

Vanossi, M. (1980), Les unités géologiques des Alpes Maritimes entre l'Ellero et la Mer Ligure: un aperçu schématique. *Memorie di Scienze Geologiche dell'Università di Padova*, 34, 101-142.

Verschure, R.H., P. A. M. Andriessen, N. A. I. M. Boelrijk, E. H. Hebeda, C. Maijer, H. N. A. Priem, E. A. Th. Verdurmen (1980), On the thermal stability of Rb-Sr and K-Ar biotite systems: evidence from coexisting Sveconorwegian (ca 870 Ma) and Caledonian (ca 400 Ma) biotites in SW Norway. *Contributions to Mineralogy and Petrology*, 74, 245-252.

FIGURE CAPTIONS

Fig. 1: (A) Location and (B) structural map of the Ligurian Alps, from *Vanossi* [1991], modified. Box indicates location of the Case Tuberto-Calizzano unit, details in the related geological map of Fig. 2. (C) Structural section through the Ligurian Alps, illustrating the position of the study area in the nappes pile, modified from *Bonini* et al. [2010].

Fig. 2: (A) Paleogeographic reconstruction of the Alpine Tethys during Late Jurassic [see Decarlis et al., in press] (B) Simplified cross section across the Alpine Tethys illustrating the main alpine palaeogeographic structural domains and rifting domains [from *Decarlis* et al., 2015](detachment faults in green).

Fig. 3: Geological map of the Case Tuberto-Calizzano unit and samples locations, modified from *Seno et al*., [2005a; 2005b.]

Fig. 4: (A, B): Scravaion schist in the Type location (see Fig.2), showing pervasive alpine deformation and related folded quartz veins network. (C, D): Quartz veins associated with widespread chlorite concentrations in the Orthogneiss I at the top of Case Tuberto Calizzano basement unit. (E, F): Silicified breccia level lying on top of the orthogneiss near Calizzano village. Orthogneiss clasts are hardly distinguishable due to the perasive silicification. Anastomosing carbonate clasts are locally associated to chlorite concentrations (F).

Fig. 5: Microphotographs in transmitted light of the selected thin sections illustrating the main petrographic features of the different lithologies of the Case Tuberto-Calizzano basement. (A-B) Plain polarized views of post-Variscan assemblages in amphibolites. (A) Pumpellyite and phengite, mimetic on the Variscan schistosity in leucocratic band. (B) Static blastesis of stilpnmomelane and pumpellyite on hornblende + oligoclase Variscan

assemblage. (C) Cross polarized view of the two generations of white mica (Wm) and brown biotite (Bt) in the two-mica gneiss of the “Gneiss-amphibolite complex”. The older generation consists of large, deformed flakes (abbreviations in italic) locally defining a old foliation oriented ca. NNE-SSW in the picture. The younger generation consists of medium-grained lepidoblasts defining the main foliation oriented ca. NE-SW in the picture. (D) Cross polarized view of an “Orthogneiss I” in which the main foliation is defined by brown biotite (Bt), white mica (Wm) and quartz ribbons (Qz). An older generation of biotite (in italic) is wrapped around by the main foliation. (E) Cross polarized view of an “Orthogneiss I” showing a K-feldspar (Kfs) rimmed by plagioclase (Pl) and myrmekites (myrm). (F) Cross polarized view of an “Orthogneiss II” in which a porphyroclastic K-feldspar (Kfs) including magmatic quartz (Qz) and brown biotite (Bt), is wrapped around by the main Variscan foliation defined by brown biotite.

Fig. 6: Microphotographs in transmitted light of the selected thin sections illustrating the post-Variscan growth of green biotite in the two-mica gneiss of the “Gneiss amphibolite complex”. Plain (A) and cross polarized (B) view showing coarse-grained white mica (Wm) and brown biotite (Bt) defining the Variscan main foliation. Both the partial recystallization of white mica into fine-grained flakes (FWm) and the local neo-formation of aggregates of fine-grained green biotite (GBt; detail in D) are recognizable. Chlorite (Chl), where present, is related to late fractures. (C) Plain polarized view of a flake of brown biotite (Bt) partly replaced by green biotite (GBt) and, at the rim, by chlorite (Chl). (E) Plain polarized view of the Variscan brown biotite (Bt) and of the younger green biotite flakes (GBt), partly replaced by chlorite (Chl), along a micro-shear zone (detail in the back-scattered image in G). (F) Back-scattered image of the green biotite flakes (GBt) partly replaced by and aggregate of chlorite (Chl). (H) Compositions of both the brown and green biotite plotted in the TiO_2/Mg vs FeO_{tot} diagram [*Engel & Engel*, 1960].

Fig. 7: Zircon fission-track and (U-Th)/He ages: samples are ordered according to their location from N to S. The distributions of the zircon fission-track ages are also shown as histogram and as population density function (PDF) curves. The zircon fission-track central ages overlap within the standard errors with the exception of samples MB1405, which is younger only if the **1σ** error is considered. Within the **2σ** error of the central ages, there is no significant difference. The (U-Th)/He ages show a large scatter which relates to incomplete age reset during the Alpine metamorphic overprint, to the large range of the eU content (Fig. 9A) and of the grain dimensions.

Fig. 8: Radial plot and Probability-Density (PD) plot showing best-fit peaks from Binomfit (Brandon [2002], version 1.2.63 (2007)) for the pooled ages of all samples (all grains). y is the **2σ** standard error of the central age of the pooled grains. At least three age populations at 129, 156 and 215 Ma characterize the age distribution of the 196 zircons of the pooled samples.

Fig. 9: (A) Negative date-eU correlation of the analysed samples. Individual points in each dataset represent single ages (2 sigma error). B) Positive date-grain size (Rs= 3*Volume/Surface) correlation. C) ZHe thermochronometric inverse modeling results of samples MB1402-04. Acceptable time-temperature paths (green area) and best fit solution (black line) determined by Hefty program [Ketcham, 2005] using the initial constrains of the ZFT ages (this study) and Jurassic-Eocene depositional age of the basement cover (Vanossi et al., 1986).

Fig. 10: Supposed location of the sampling sites within Case Tuberto-Calizzano unit during the Alpine Tethys rifting, and suggested tectonic evolution within the distal margin, modified from *Decarlis et al.* [2015]. (A) Upper Sinemurian-Pliensbachian stage: the distal margin was progressively thinned and became tectonically active. The Briançonnais

domain was uplifted under subaerial conditions while Prepiedmont domain, separated by the φ fault system, remained in submerged and progressively drowning marine environment. (B) Late Jurassic stage stage: after subcontinental mantle exhumation at the seafloor through the ε detachment fault system (Ligurian-Penninic domains), Briançonnais subsided and tectonics ceases along the distal margin.

Table captions

Tab. 1: Zircon fission track data

Tab. 2: Zircon (U-Th)/He data

Figure 1.

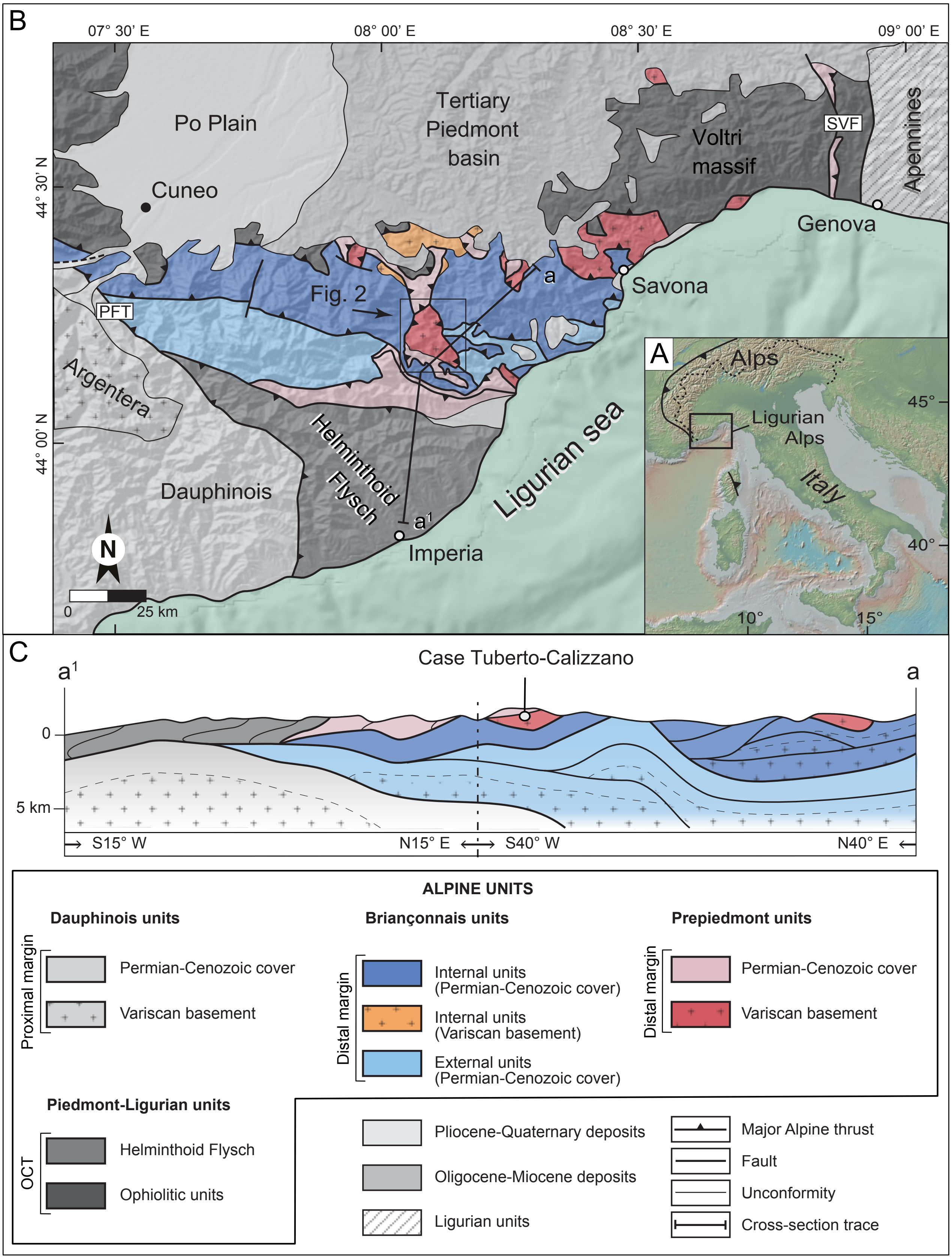
B
07° 30' E
08° 00' E
08° 30' E
09° 00' E
44° 30' N
44° 00' N
Po Plain
Cuneo
Tertiary
Piedmont
basin
Voltri
massif
SVF
Apennines
Genova
Savona
a
Fig. 2
PFT
Argentera
Dauphinois
Helminthoid
Flysch
a1
Imperia
Ligurian sea
N
0
25 km
A
Alps
Ligurian
Alps
Italy
45°
40°
10°
15°
C
Case Tuberto-Calizzano
a1
a
0
5 km
S15° W
N15° E
S40° W
N40° E
ALPINE UNITS
Dauphinois units
Proximal margin
Permian-Cenozoic cover
Variscan basement
Briançonnais units
Distal margin
Internal units
(Permian-Cenozoic cover)
Internal units
(Variscan basement)
External units
(Permian-Cenozoic cover)
Prepiedmont units
Distal margin
Permian-Cenozoic cover
Variscan basement
Piedmont-Ligurian units
OCT
Helminthoid Flysch
Ophiolitic units
Pliocene-Quaternary deposits
Oligocene-Miocene deposits
Ligurian units
Major Alpine thrust
Fault
Unconformity
Cross-section trace

Figure 2.

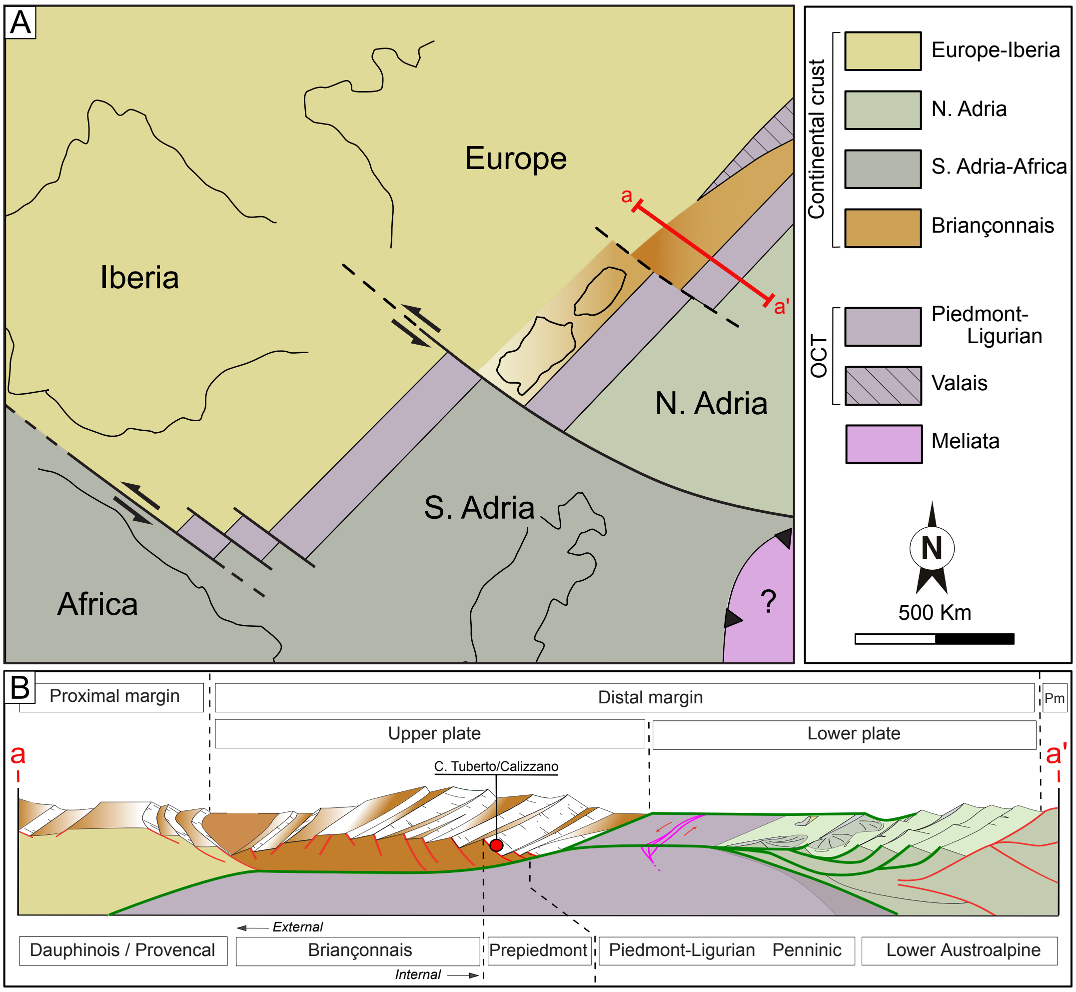
A
Europe
Iberia
N. Adria
S. Adria
Africa
a
a'
?
Continental crust
Europe-Iberia
N. Adria
S. Adria-Africa
Briançonnais
OCT
Piedmont-Ligurian
Valais
Meliata
N
500 Km
B
Proximal margin
Distal margin
Pm
Upper plate
Lower plate
a
a'
C. Tuberto/Calizzano
External
Internal
Dauphinois / Provencal
Briançonnais
Prepiedmont
Piedmont-Ligurian Penninic
Lower Austroalpine

Figure 3.

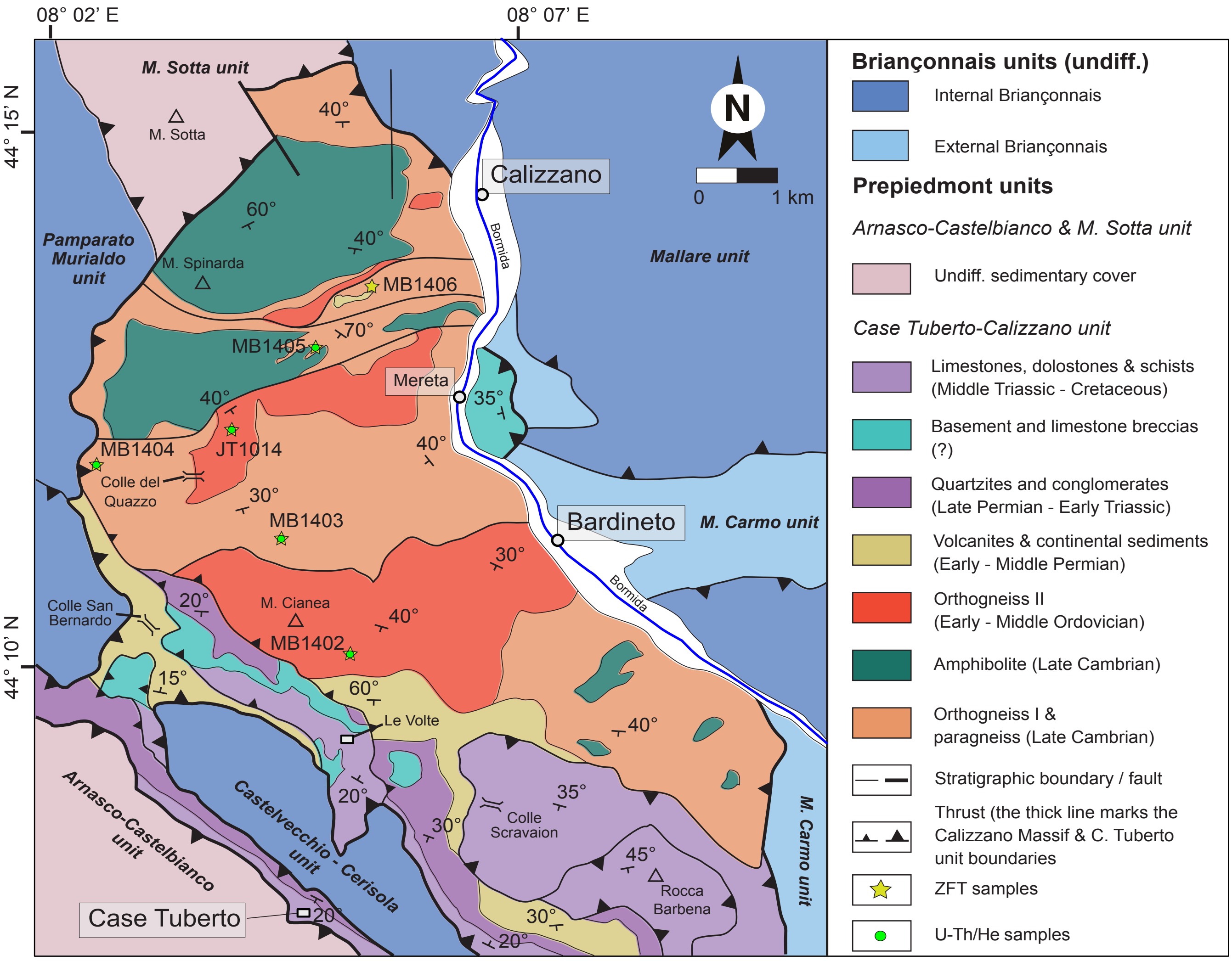

08° 02' E
08° 07' E
44° 15' N
44° 10' N
M. Sotta unit
M. Sotta
Pamparato Murialdo unit
M. Spinarda
Calizzano
Bormida
Mallare unit
MB1406
MB1405
Mereta
JT1014
MB1404
Colle del Quazzo
MB1403
Bardineto
M. Carmo unit
Colle San Bernardo
M. Cianea
MB1402
Le Volte
Colle Scravaion
Rocca Barbena
Arnasco-Castelbianco unit
Castelvecchio - Cerisola unit
Case Tuberto
N
0
1 km
Briançonnais units (undiff.)
Internal Briançonnais
External Briançonnais
Prepiedmont units
Arnasco-Castelbianco & M. Sotta unit
Undiff. sedimentary cover
Case Tuberto-Calizzano unit
Limestones, dolostones & schists (Middle Triassic - Cretaceous)
Basement and limestone breccias (?)
Quartzites and conglomerates (Late Permian - Early Triassic)
Volcanites & continental sediments (Early - Middle Permian)
Orthogneiss II (Early - Middle Ordovician)
Amphibolite (Late Cambrian)
Orthogneiss I & paragneiss (Late Cambrian)
Stratigraphic boundary / fault
Thrust (the thick line marks the Calizzano Massif & C. Tuberto unit boundaries
ZFT samples
U-Th/He samples

Figure 4.

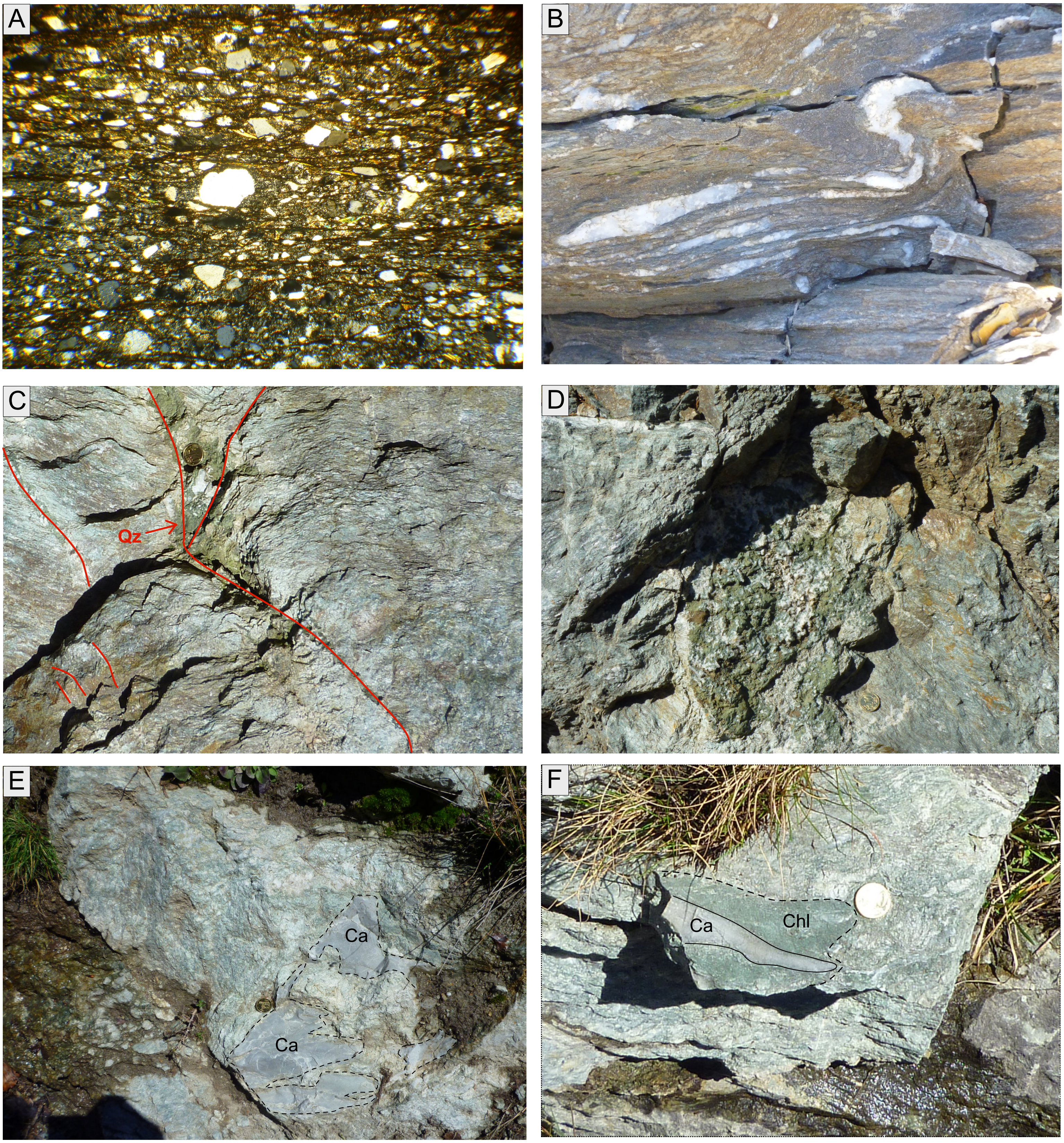
A
B
C
Qz
D
E
Ca
Ca
F
Ca
Chl

Figure 5.

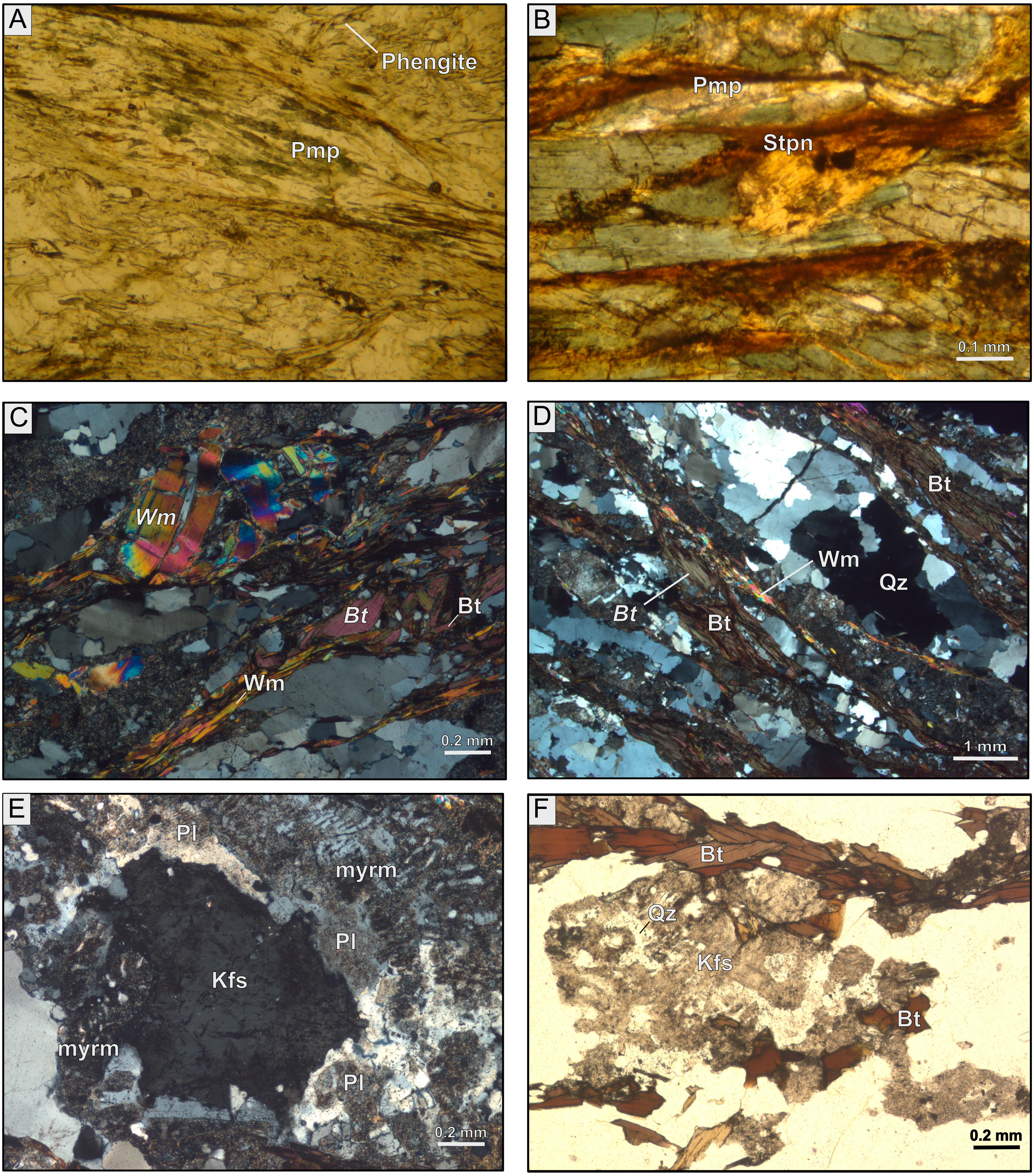
A
Phengite
Pmp
B
Pmp
Stpn
0.1 mm
C
Wm
Bt
Bt
Wm
0.2 mm
D
Bt
Wm
Qz
Bt
Bt
1 mm
E
Pl
myrm
Pl
Kfs
myrm
Pl
0.2 mm
F
Bt
Qz
Kfs
Bt
0.2 mm

Figure 6.

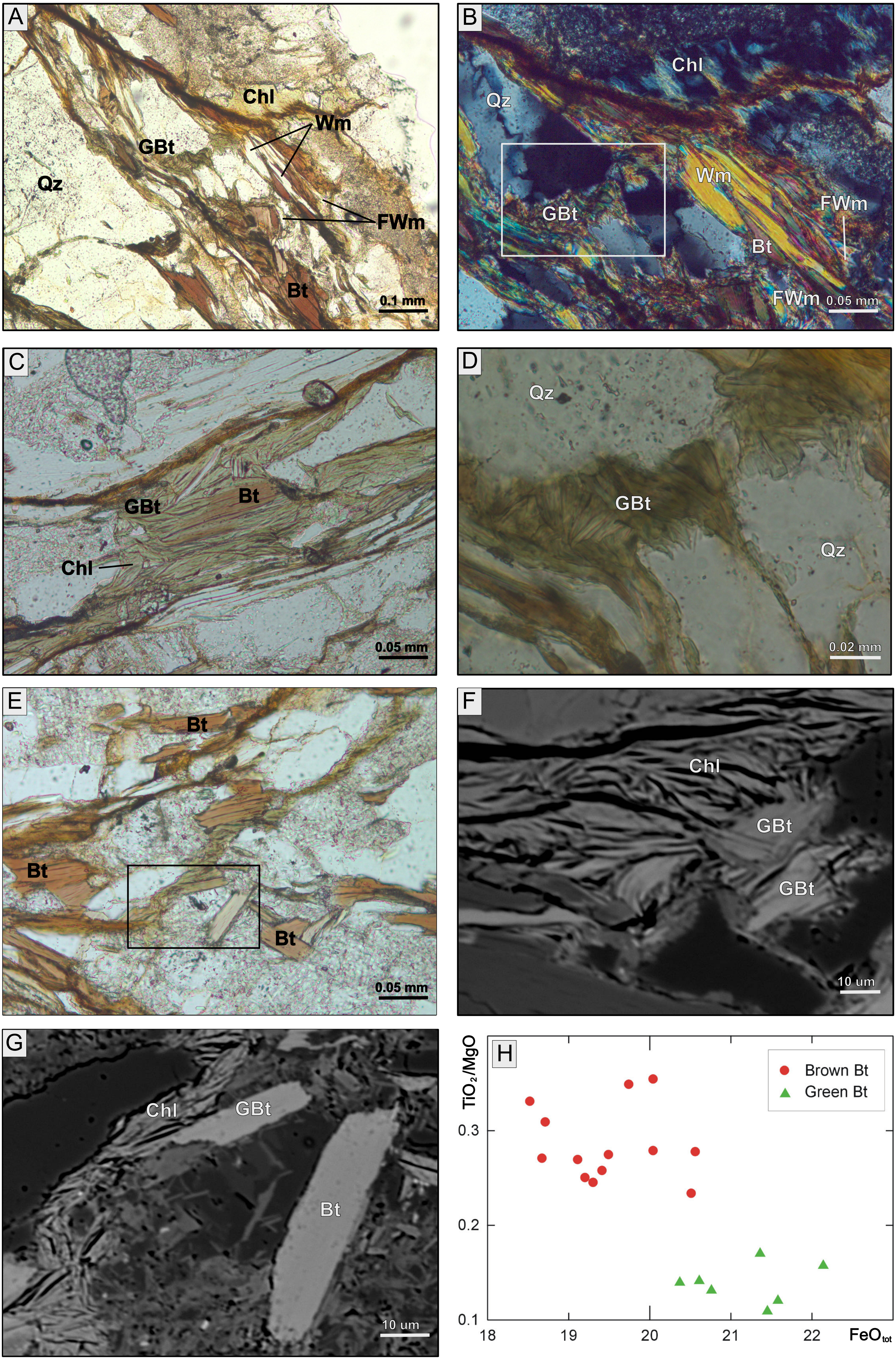
A
Chl
Wm
GBt
Qz
FWm
Bt
0.1 mm
B
Chl
Qz
Wm
GBt
FWm
Bt
FWm
0.05 mm
C
Bt
GBt
Chl
0.05 mm
D
Qz
GBt
Qz
0.02 mm
E
Bt
Bt
Bt
0.05 mm
F
Chl
GBt
GBt
10 um
G
Chl
GBt
Bt
10 um
H
TiO2/MgO
FeOtot
Brown Bt
Green Bt
0.1
0.2
0.3
18
19
20
21
22

Figure 7.

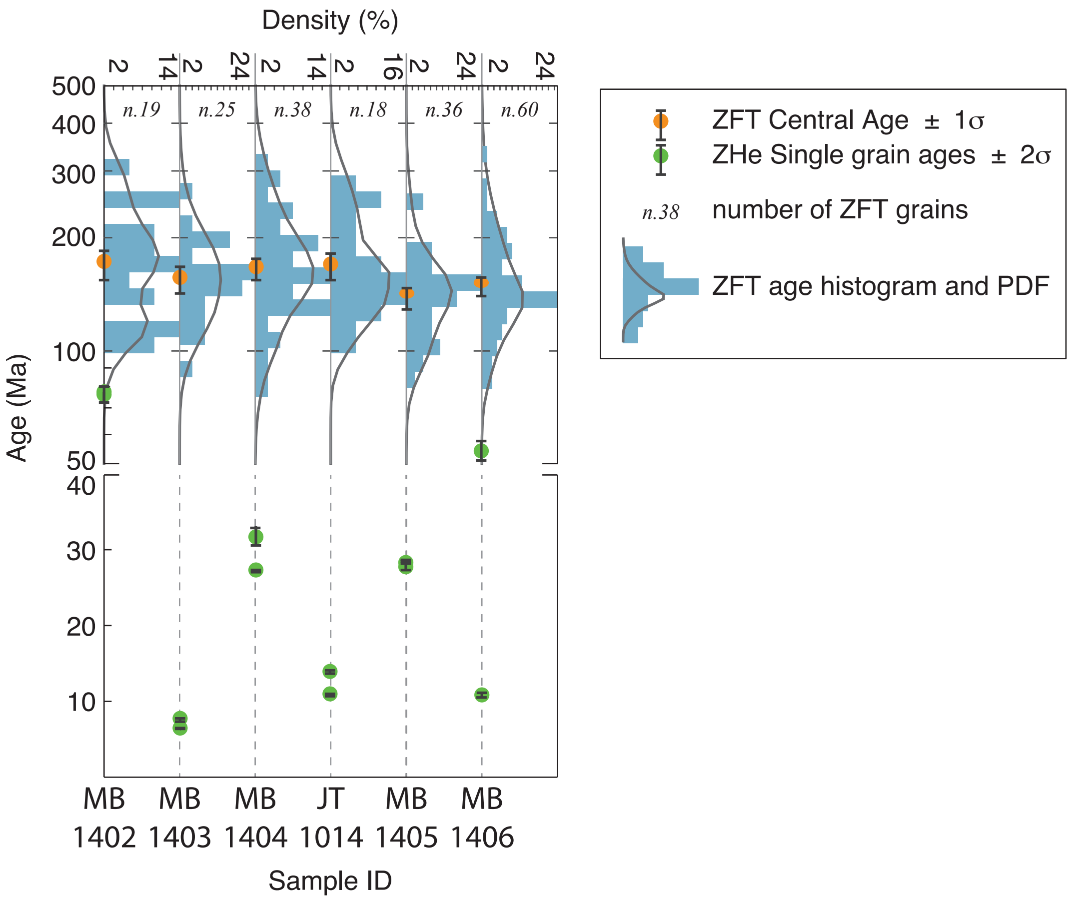

Density (%)
2
14
2
24
2
14
2
16
2
24
2
24
n.19
n.25
n.38
n.18
n.36
n.60
500
400
300
200
100
50
40
30
20
10
Age (Ma)
MB 1402
MB 1403
MB 1404
JT 1014
MB 1405
MB 1406
Sample ID
ZFT Central Age ± 1σ
ZHe Single grain ages ± 2σ
n.38
number of ZFT grains
ZFT age histogram and PDF

Figure 8.

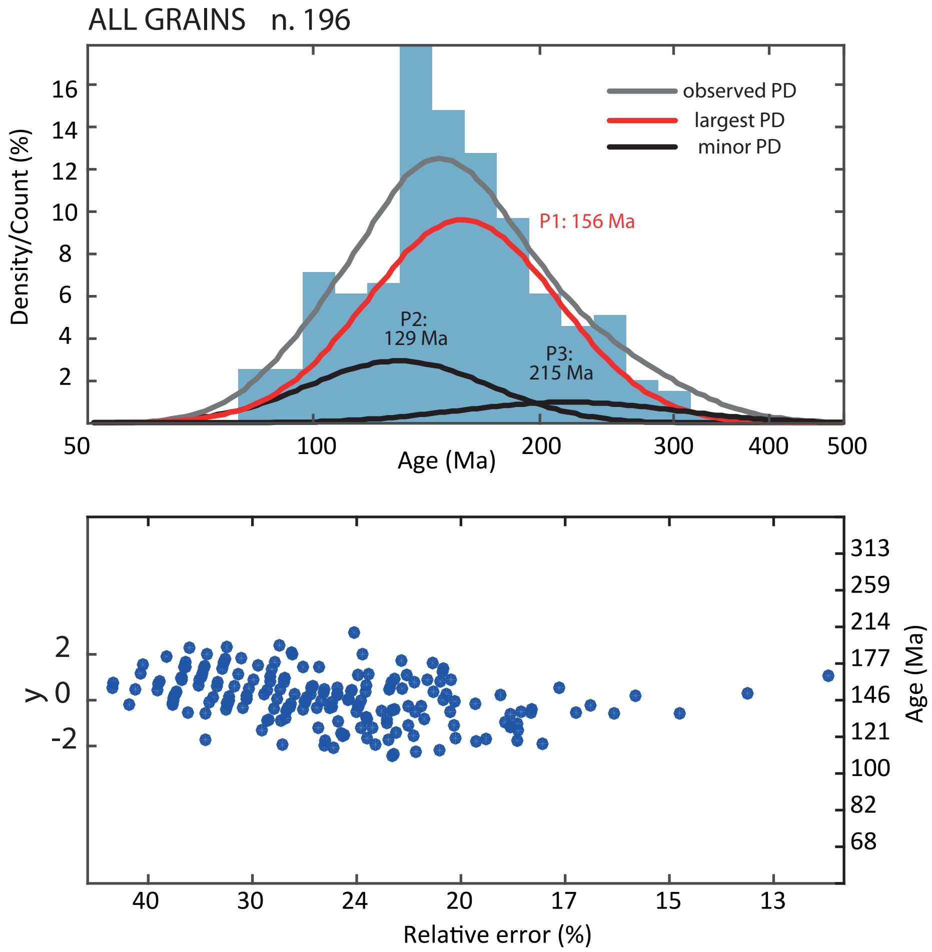

ALL GRAINS n. 196
Density/Count (%)
16
14
12
10
8
6
4
2
observed PD
largest PD
minor PD
P1: 156 Ma
P2:
129 Ma
P3:
215 Ma
50
100
200
300
400
500
Age (Ma)
2
y 0
-2
313
259
214
177
146
121
100
82
68
Age (Ma)
40
30
24
20
17
15
13
Relative error (%)

Figure 9.

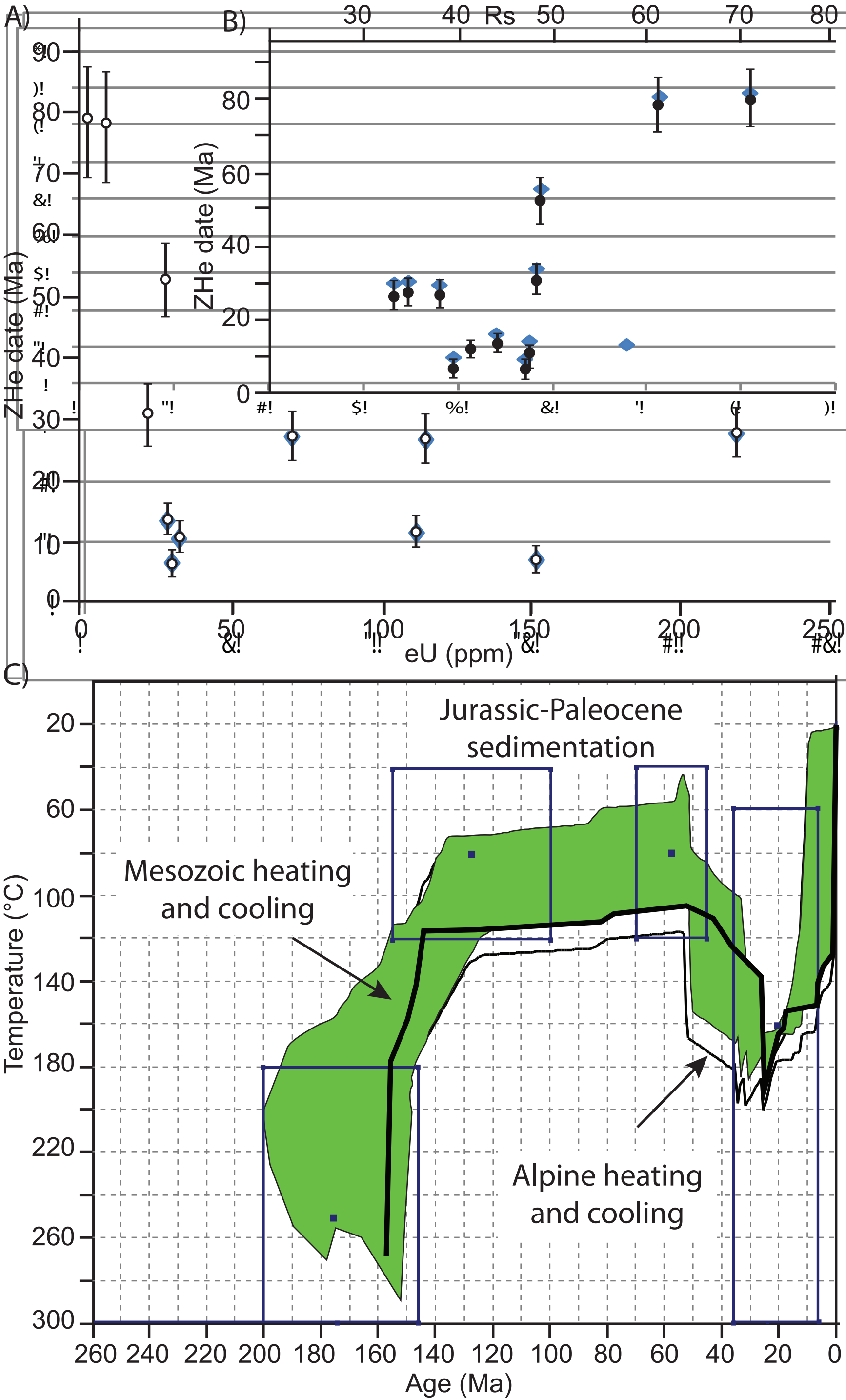
A)
B)
C)
Rs
ZHe date (Ma)
eU (ppm)
Jurassic-Paleocene
sedimentation
Mesozoic heating
and cooling
Alpine heating
and cooling
Temperature (°C)
Age (Ma)

Figure 10.

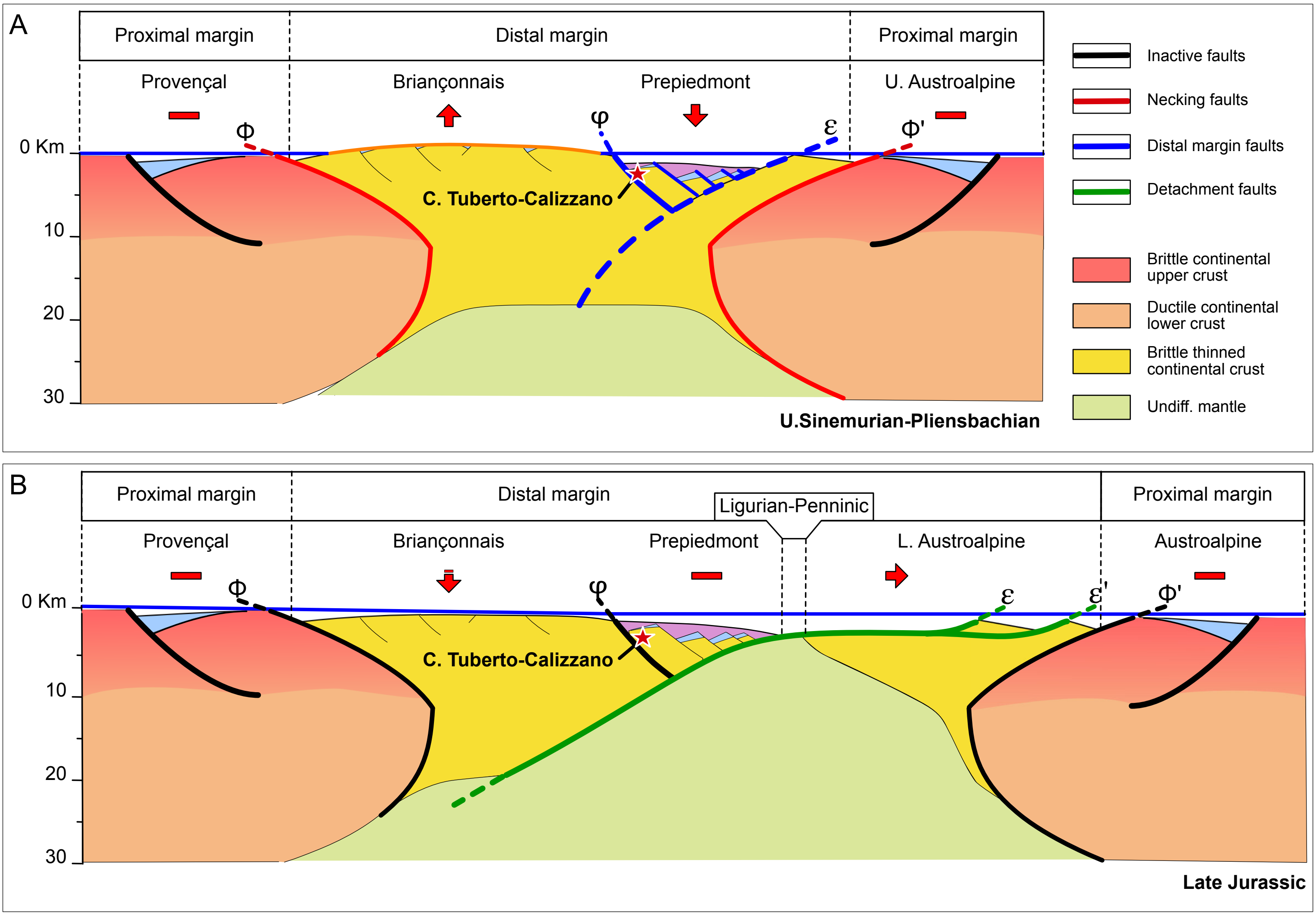
A
Proximal margin
Distal margin
Proximal margin
Provençal
Briançonnais
Prepiedmont
U. Austroalpine
Φ
φ
ε
Φ'
0 Km
10
20
30
C. Tuberto-Calizzano
U.Sinemurian-Pliensbachian
Inactive faults
Necking faults
Distal margin faults
Detachment faults
Brittle continental upper crust
Ductile continental lower crust
Brittle thinned continental crust
Undiff. mantle
B
Proximal margin
Distal margin
Ligurian-Penninic
Proximal margin
Provençal
Briançonnais
Prepiedmont
L. Austroalpine
Austroalpine
Φ
φ
ε
ε'
Φ'
0 Km
10
20
30
C. Tuberto-Calizzano
Late Jurassic

Sample / mount	Location Lat	Long	Elevation (m)	Gr.	N_d track	ρ_d 1E+05 track/cm^2	N_s track	ρ_s 1E+07 track/cm^2	N_i track	ρ_i 1E+06 track/cm^2	P(X^2) %	Age dispersion %	Pooled Age ± σ1 Ma	Central Age ± σ1 Ma	Pop Age -LCI +Ucl Ma	Fraction of Gr. %	Age range
MB1402/a	44°10'36"	8°05'03"	1030	9	5277	3.9129	2303	1.5846	382	2.6283	1.75	20.53	168.6 ± 9.7	168.0 ± 14.9			103.8 - 300.8
MB1402/b				10	5238	3.8834											
MB1403/b	44°11'29"	8°04'55"	990	10	5158	3.8243	2051	1.7272	365	3.0737	74.85	1.67	153.4 ± 9.1	153.6 ± 11.6			94.5 - 271.8
MB1403/c				15	5118	3.7948											
MB1404/a	44°12'07	8°03'05"	970	38	5078	3.7653	4398	1.2824	726	2.1170	3.93	14.49	163.6 ± 7.0	163.8 ± 11.2			83.2 – 313.2
JT1014/b	44°12'40	8°04'21"	925	9	4779	3.5586	2474	1.2712	379	1.9474	22.34	8.77	165.9 ± 9.6	166.2 ± 13.0			107.6 – 292.3
JT1014/c				9	4760	3.5291											
MB1405/a	44°13'21	8°05'20"	800	24	4999	3.7062	3943	1.1781	759	2.2677	56.28	1.16	138.1 ± 5.8	138.1 ± 8.8			86.4 – 253.1
MB1405/b				12	4959	3.6767											
MB1406/a				30	4919	3.6472	6141	1.2204	1088	2.1622	19.66	9.14	147.3 ± 5.2	147.5 ± 9.0	117.5 -68.0 +159.1	7	85.3 - 339.0
MB1406/b				30	4879	3.6176									150.6 -15.2 +17.0	93	
ALL				196											128.7 -32.9 - +41.1 156.2 -32.9 +41.5 214.9 -43.5 +54.3	21 71 8	
ζ calibration factor: 145.39 ± 7.04																	

Sample/ Aliquot	Location		Elevation (m)	Mean grain radius – Rs (µm)	U (ng)	Th (ng)	4He (ncc)	eU (ppm)	Analytical error %	Raw age (Ma)	Th/U	FT	Corrected age (Ma)
	Lat	**Long**											
MB1402/1	44°10'36"	8°05'03"	1030	61.5	2,74	0,36	2,1E-08	7,50	3,11%	60,4	0.13	0.78	77.4
MB1402/2				71.0	1,06	0,23	8,6E-09	2,01	5,06%	62,8	0.21	0.80	78.5
												Mean ZHe Age	**78 ± 9.3**
MB1403/1	44°11'29"	8°04'55"	990	47.1	4,05	1,05	2,4E-09	28,90	1,19%	4,6	0.26	0.72	6.6
MB1403/2				39.5	14,61	0,45	9,4E-09	151,69	2,50%	5,3	0.03	0.69	7.3
												Mean ZHe Age	**6.9± 0.8**
MB1404/1	44°12'07"	8°03'05"	970	38.2	9,15	2,95	2,2E-08	114,08	0,60%	18,5	0.32	0.68	26.8
MB1404/2				48.3	3,71	0,14	1,1E-08	21,67	7,64%	23,4	0.04	0.74	31.2
												Mean ZHe Age	**29.0 ± 3.4**
JT1014/1	44°12'40"	8°04'21"	925	44.1	3,58	0,67	4,6E-09	27,82	1,75%	10,0	0.19	0.72	13.5
JT1014/2				47.5	17,21	2,86	1,8E-08	111,66	0,59%	8,1	0.17	0.74	11.6
												Mean ZHe Age	**12.6 ± 1.5**
MB1405/1	44°13'21"	8°05'20"	800	33.4	3,73	0,65	8,5E-09	69,23	1,79%	18,0	0.17	0.65	26.9
MB1405/2				34.8	13,14	1,95	3,1E-08	218,71	0,72%	18,7	0.15	0.66	27.5
												Mean ZHe Age	**27.2 ± 3.2**
MB1406/1	44°13'49"	8°05'56"	880	42.9	7.36	8.38	9,2E-09	31,79	4.09%	8.1	1.14	0.70	11.6
MB1406/2				48.8	4.59	0.69	2,3E-08	27,03	1.67%	39.6	0.15	0.75	52.8
													n.d.
FCT/1				40.4	2,11	1,29	5,2E-09		1,61%	17,6	0.61	0.68	25.9
FCT/1				65.9	1,99	1,41	7,2E-09		1,60%	25,6	0.71	0.80	32.0
												Mean ZHe Age	**29.0 ± 3.4**

[a] Single crystal aliquots were used for all samples. U and Th data are corrected for a procedural blank of 0.1067 ng U and 0.0997 ng Th. Blank uncertainty is ± 10% and is included in the analytical uncertainty. The main grain radius (Rs) is derived from the Mass Weighted Average Radius (MWAR). eU is the effective uranium content computed as [U] + 0.235[Th]. ZHe ages are corrected for the recoil correction, F_T, calculated using the calculations of Ketcham et al. (2011) assuming homogeneity. FCT is the Fish Canyon Tuff standard. Age uncertainties from ZHe age measurement are 11.9% (calculated from the 2σ age reproducibility of the FCT age standard).